Modular Modification of a Buoyant AUV for Low-Speed Operation

By: Christopher Lee Nickell

Thesis submitted to the Faculty of the
Virginia Polytechnic Institute and State University
in partial fulfillment of the requirements for the degree of

Master of Science
in
Aerospace Engineering

Dr. Craig Woolsey, Committee Chair
Dr. Hanspeter Schaub, Committee Member
Dr. Daniel Stilwell, Committee Member

September 9, 2005
Blacksburg, Virginia

Keywords: Internal Actuation, Moving Mass, AUV, Autonomous Underwater Vehicle

Modular Modification of a Buoyant AUV for Low-Speed Operation

Christopher Lee Nickell

Abstract

Conventional streamlined autonomous underwater vehicles (AUVs) with a single thruster and stern planes are typically trimmed to be somewhat buoyant or heavy in water. To maintain depth, they must generate a constant hydrodynamic force which requires that they swim at a constant pitch angle. Although tail fins are the typical mechanism for generating this control moment, they become ineffective at low speeds. To enable an existing AUV to travel at lower speeds, one may easily incorporate a modular moving mass actuator. In some cases, it may also be advantageous to include a fixed wing.

The equations of motion and equilibrium conditions to regulate depth are derived, and the effectiveness and low-speed efficiency of a fixed wing is evaluated. The effect of the vertical offset of the moving mass is analyzed to establish the relation between the control angle and the moving mass linear position.

A description of the design of a one degree of freedom moving mass actuator module and preliminary experiments using the Virginia Tech Miniature AUV is provided. Data is presented for a series of fixed MMA position experiments as well as a dynamic position test. The results illustrate the effectiveness of a moving mass actuator at generating low-speed control moments. With the collected data, parameter identification is performed to get an estimate of the hydrodynamic parameters.

Acknowledgments

Deep appreciation is given to Dr. Craig Woolsey for his time and guidance over the course of this thesis. With his help and patience this research was possible. I thank the Virginia Tech Aerospace and Ocean Engineering Faculty, James Lambert, Bruce Stanger and Stephen Edwards for their wisdom and time in the creation of the MMA. I thank Dr. Daniel Stilwell and his Virginia Tech Miniature AUV team for their time, aid, and the use of their vehicle. Deepest appreciation is given to Dr. Hanspeter Schaub for his time and help editing this thesis. Finally, I thank my friends Konda Reddy, Amy Linklater, and Mike Morrow for their patience and help during the writing of this thesis.

Contents

List of Figures

List of Tables

Notation

Shorthand	
AC	Aerodynamic center
GEO	Geometric center of pressurized wing-body
CB	Center of buoyancy of pressurized hull
CG	Center of gravity of AUV
$Newt$	Newtonian theory
SB	Slender-body theory
Environment	
ρ	Fluid density
g	Gravitational acceleration
Lengths	
L	Overall hull length
X	reference length for dimensionalization
L_t	distance from the aerodynamic force center of the hull to the aerodynamic force center of the horizontal tail
r	Hull cylindrical radius
s	Wing half-span
x_{ac}	distance from nose to aerodynamic force center
x_c	distance from nose to centroid of the body planform area
x_m	distance from the nose to the pitching-moment reference center
$\boldsymbol{r_{cg}}$	location of center of gravity from GEO in body coordinates, $\left[r_{cg_x}, r_{cg_y}, r_{cg_z}\right]$
$\boldsymbol{r_p}$	location of moving mass from GEO in body coordinates, $\left[r_{p_x}, r_{p_y}, r_{p_z}\right]$

Angles	
α	Angle of Attack, AoA, Angle between body x and velocity x
α_f	Angle of Attack as seen from horizontal tail
γ	Glide path angle, Angle between inertial x and velocity x
θ	Pitch angle, Angle between inertial x and body x
Areas	
A_b	body base area (at $x = L$)
A_p	body planform area
A_r	body reference area
A_t	fin surface/reference area
Velocity	
$\boldsymbol{v}$	Body translational velocity vector defined as $[u, v, w]^T$
V_∞	free stream velocity, $\|\boldsymbol{v}\|$
$\boldsymbol{\Omega}$	Body angular velocity vector defined as $[p, q, r]^T$
$\bar{\boldsymbol{v}}$	Body translational and angular velocity vector defined as $\left[\boldsymbol{\Omega}^T, \boldsymbol{v}^T\right]^T$
Mass	
m_p	moving point mass
m_b	body mass at vehicle center of gravity without moving mass
m_{buoy}	mass of displaced fluid volume
M_{f_x}	added mass in the body x direction
M_{f_y}	added mass in the body y direction
M_{f_z}	added mass in the body z direction
$\boldsymbol{M_f}$	added fluid mass matrix in the body frame $diag\left[M_{f_x}, M_{f_x}, M_{f_x}\right]^T$
$\boldsymbol{I_b}$	body moment of inertia matrix centered on GEO
	in the body frame
I_{f_x}	added inertia in the body roll direction
I_{f_y}	added inertia in the pitch direction
I_{f_z}	added inertia in the yaw direction
$\boldsymbol{I_f}$	added fluid inertia matrix in the body frame $diag\left[I_{f_x}, I_{f_x}, I_{f_x}\right]^T$

Forces	
B	Vehicle buoyancy
W_{total}	Vehicle total weight
L_{wb}	Lift of the wing-body expressed in the velocity frame
L_t	Lift of the tail expressed in the velocity frame
D_{wb}	Drag of the wing-body expressed in the velocity frame
D_{ht}	Drag of the tail expressed in the velocity frame
N_{wb}	Normal force of the wing-body expressed in the body frame
N_{ht}	Normal force of the tail expressed in the body frame
A_{wb}	Axial force of the wing-body expressed in the body frame
A_{ht}	Axial force of the tail expressed in the body frame
N_t	Total normal force, $N_{wb} + N_{ht}$
A_t	Total axial force, $A_{wb} + A_{ht}$
T	Thrust force assumed centered on the body x axis
Moments	
$\boldsymbol{M_{cg}}$	moment generated from a noncoincident CG, $\boldsymbol{r_{cg}} \times m_b g \boldsymbol{R}^T [0\ 0\ 1]^T$
$\boldsymbol{M_{wb}}$	moment generated from an offset AC, $\boldsymbol{r_{AC}} \times \boldsymbol{R_{BF}} [A_t\ 0\ N_t]^T$
$\boldsymbol{M_p}$	static moment generated by moving mass, $\boldsymbol{r_p} \times m_p g \boldsymbol{R}^T [0\ 0\ 1]^T$
$\boldsymbol{M_{ext}}$	external torque expressed in the body frame
Nondim	
C_{d_n}	crossflow drag coefficient of a circular cylinder section
η	crossflow drag proportionality factor
$C_{N_{wb}}$	nondimensional normal force coefficient of the wing-body, $\frac{N_{wb}}{\bar{q} A_r X}$
$C_{N_{ht}}$	nondimensional normal force coefficient of the horizontal tail, $\frac{N_{ht}}{\bar{q} A_r X}$
$C_{D_{wb_0}}$	overall net drag coefficient of wing-body in a straight and level zero deflection condition.
$C_{D_{f_0}}$	overall net drag coefficient of the fins in a straight and level zero deflection condition
$C_{A_{wb}}$	nondimensional axial force coefficient of the wing-body, $\frac{A_{wb}}{\bar{q} A_r X}$
$C_{A_{ht}}$	nondimensional axial force coefficient of the horizontal tail, $\frac{A_{ht}}{\bar{q} A_r X}$
$C_{m_{wb}}$	pitching moment coefficient, referenced x_m from nose, $\frac{pitching\ moment}{\bar{q} A_r X}$
AR_{fin}	fin aspect ratio
$\frac{L}{r}$	vehicle slenderness ratio
$\frac{s}{r}$	wing protrusion ratio ($\frac{s}{r} = 1$ for No Wings)
$\frac{B}{W}$	buoyancy factor (Buoyant > 1, Heavy < 1)
$\forall_t$	horizontal tail volume ratio, $\left(\frac{L_t}{L}\frac{A_t}{A_p}\right)$

Chapter 1

Introduction

Autonomous underwater vehicles (AUVs) are typically trimmed to be slightly heavy or buoyant. A constant force must be generated to counteract the excess gravitational or hydrostatic force in order to maintain depth (Fig. 1.1). This force is generated through

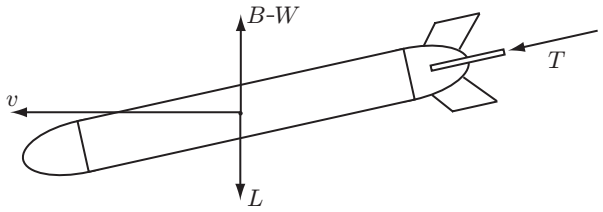

Figure 1.1: A constant downward force is generated to counteract the vehicle positive buoyancy allowing depth regulation

direct propulsion or through use of the body hydrodynamic lift. Using the body lift requires the AUV to travel at a constant angle of attack (AoA). The tail fins are used to generate the necessary moment to maintain the proper AoA but fail at low speed. A modular moving mass actuator (MMA) can be used to supplement the pitch control in these conditions. In addition to pitch supplementation, a fixed wing can be used to lower the operating speed or increase the low-speed efficiency of an AUV by increasing the effectiveness of the wing-body hydrodynamics.

This thesis will examine alternative methods of attitude control for a positively buoyant streamlined AUV with a conventional single thruster and stern planes, and describe the design and implementation of a modular moving mass actuator and wing for pitch and depth control.

1.1 Mission

The vehicle velocity and the necessary control to achieve that velocity is set by the intended mission of the AUV. The complexity and cost of an autonomous system places high priority on recoverability in the event of a failure. Designing the vehicle to be positively buoyant ensures vehicle recovery in the event of a mechanical failure or software flaw. Unfortunately, the introduction of this requirement imposes a constant hydrostatic force that must be countered for depth regulation. This net buoyancy force is offset through the use of additional thrusting or manipulation of the wing-body hydrodynamics (i.e. downward lift) or both.

As velocity decreases, the vehicle hydrodynamic forces begin to wain. To counteract the vehicle net buoyancy, the magnitude of the opposing hydrodynamic force must remain the same. This is accomplished through an increase in the vehicle angle of attack. As velocity continues to decrease, the magnitude of the angle of attack is increased until the wing-body stalls or the actuator fails to provide enough torque. This lifting force can be supplemented and stall delayed through the use of a wing. This idea is further explored in Chapter 5.

We want the vehicle to be as robust to downward velocity changes as possible. The vehicle top speed is set by the full throttle conditions of the thruster where the lower velocity limit is the point where depth can no longer be maintained. It is not possible to expand this point all the way to zero without additional direct forcing or a reballasting of the vehicle, however extending the minimum speed as low as possible will allow slow passes of a target or stationkeeping in the presence of a current. An AUV capable of this type

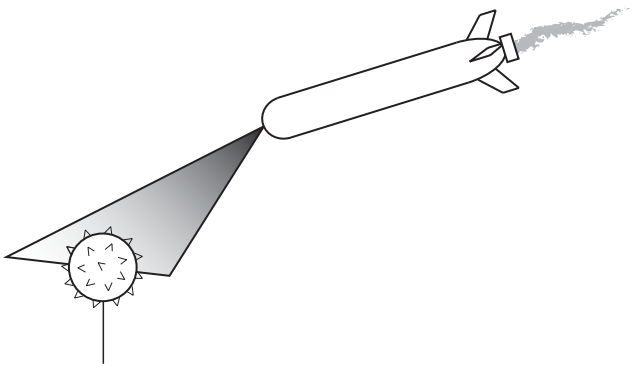

Figure 1.2: Ordnance inspection, mapping, or safe detonation

of maneuver can be used for mine identification and disposal or can be used in harbors to inspect the hulls of ships for damage or contraband. As the AUV matures the positive buoyancy requirement may be relaxed opening the vehicle to new missions. If reballasted

to neutral buoyancy, the AUV might require a large range of pointing accuracy for highly directional sensors. This allows object identification and inspection using sonar or vision based sensors. Adding wings and a variable ballast system transforms an AUV into an energy efficient underwater glider.

1.2 History

To understand low-speed control of an AUV we must first explore previous research conducted in the development of this class of vehicle. The first appearance of an AUV-like device can be traced back to Whitehead Automobile "Fish" Torpedoes [1] in Austria in 1866. This device carried an 18 pound explosive charge and was driven by compressed air, achieving a speed exceeding 3.0 $\frac{m}{s}$ over 700 m.

The first true research AUV rose from the need to study arctic underice profiles in the late 1950s. The Self Propelled Underwater Research Vehicle (SPURV) was developed by Stan Murphy, Bob Francois, and Terry Ewart of the University of Washington's Applied Physic Laboratory. SPURV I became operational in the early 1960s and operated at 2.2 $\frac{m}{s}$ for 5.5 hours at a depth of 3 km. SPURV communicated acoustically with the surface and operated autonomously at constant pressure, between two depths, or at a constant climb or dive angle. Data was taken at constant pressure areas to support wave modelling [2]. The same vehicle was later used to track horizontal and vertical dye dispersion at depths up to 1 km for up to 66 hours after release [3]. During the 70's and 80's SPURV II was similarly used to study the dispersion of submarine wakes.

In response to the 1973 sinking of the USS Thresher, the USS Scorpion, and the loss of an H bomb in Palomares, the Naval Ocean Systems Center, now NRad, began development of the Advanced Unmanned Search System (AUSS). Launched in 1983, the AUSS completed over 114 dives up to a depth of 6 km. Using the newly developed acoustic communications system that was capable of transmitting video, the AUSS could search at a rate of 1.5 $\frac{nmi^2}{hr}$ with speeds up to 2.5 $\frac{m}{s}$ [4]. Additionally, the idea of a network of smaller free swimming crafts can be traced back at least this far.

The French Research Institute for Exploitation of the Sea, IFREMER, designed Epulard in 1976, deploying it in 1980. It was acoustically controlled and rated for 6 km where it supported deep ocean photography. Epulard successfully completed 300 dives between 1980 and 1990 [5].

In the late 80's and early 90's interest in AUVs began to significantly pick up. Multiple acoustically controlled untethered ROV's began to emerge through the U.S. Advanced

Research Projects and academic interest.

The Massachusetts Institute of Technology (MIT) developed six Odyssey vehicles that operated at 1.5 $\frac{m}{s}$ for up to 6 hours at a 6 km depth. These vehicles were even used under the ice in 1994 [6]. The Odyssey vehicles were networked together for a series of experiments to demonstrate the Autonomous Ocean Sampling Network [7].

The Woods Hole Oceanographic Institute (WHOI) designed and created the Autonomous Benthic Explorer (ABE) in the early 90's. This vehicle excelled in the near bottom surveying of the rugged seafloor terrain. The ABE was completely independent of the surface vessel, freeing the ship to perform other tasks outside of the acoustic range of the vehicle. It was highly maneuverable in 3 dimensions due to it's 6 thrusters. The ABE can operate up to 34 hours at depths up to 5 km and travels approximately 0.75 $\frac{m}{s}$.

On a much larger scale International Submarines Engineering, Ltd.'s vehicle Theseus displaced 8,600 kg and was developed for U.S. and Canadian defense agencies. Theseus operated at 2.0 $\frac{m}{s}$ for up to 100 hours at 1 km. In 1996 it was used to lay 190 km of fiber optic cable under ice [8].

In the late 90's WHOI introduced REMUS, an AUV displacing 36 kg, to support scientific objectives from the LEO-15 observatory in Tuckerton, NJ [9]. It could operate for 20 hours at a speed of 1.5 $\frac{m}{s}$ at up to 100 m depth. Currently their are over 50 REMUS vehicle used in research institutions all over the world including 9 universities and 3 US Navy laboratories.

The development of Autosub in the early 90's by South Hampton Oceanography Center opened the door to the long duration mission. Travelling at 1.5 $\frac{m}{s}$ Autosub had a 6 day operation time at a 1.6 km depth. In 1998 it took data at a depth of 1 km for 50 hours [10]. Autosub's high endurance specifications allowed scientists a larger temporal range of data and further inspired interest in AUV research.

In 1989 through the visionary article of Henry Stommel [11] new branch of underwater vehicles was born. These underwater gliders are AUVs that utilize a variable ballast system in conjunction with a wing to glide. This generates a component of thrust propelling the craft without the use of a conventional propulsion system. These vehicles incorporate internal actuation through a series of ballast tanks and moving masses to control the ascent/desent rate and the glide path.

The underwater glider SLOCUM, developed by Webb Research Corporation, was designed and tested in 1991. The glider was comparable in size to REMUS with a displacement of 40 kg. It achieves a horizontal flight speed of approximately 0.25 $\frac{m}{s}$ at a glide slope of 40°. The most recent version uses an energy efficient thermal ballast engine.

SLOCUM uses a battery pack on a lead screw to fine tune pitch and roll control where the majority of control is provided through the ballast tanks. Its intended missions include monitoring an ocean grid over a 5 year period, seeking out and tracking features of interest, or performing a virtual mooring by profiling the same column of water over 5 years [12].

The underwater glider Spray was developed through Scripps Institution of Oceanography in conjunction with WHOI as a low cost ($\$25,000$) research glider. Spray has a horizontal travel speed of 0.2-0.3 $\frac{m}{s}$ and communicates at the surface through satellite linkup [13]. In September 2004, Spray travelled nearly 600 miles to Bermuda crossing the gulf stream making history and taking sensory information as it travelled.

Stommel's idea quickly flourished as many universities took interest in the development of underwater gliders. The University of Washington's Seaglider [14] was developed as a high endurance oceanographic vehicle. Princeton's Rogue was designed as a laboratory scale test platform for dynamic and control research [15].

With the introduction of Spray and REMUS, the dream of an underwater network of gliders and AUVs took a step forward. Low cost miniature AUVs like the Naval Academy's USNA-1 [16] and the Virginia Tech Miniature Autonomous Underwater Vehicle (VTMAUV) [17] were created as a cost effective research vehicle capable of different missions and sensor platforms. Through modular design, a fleet of these vehicles (figure 1.3) could be deployed for use in a variety of missions reducing the overall cost of long term oceanographic projects.

All of these AUVs operate in low-speed conditions as described by a Reynolds number less than 10^7 [18] and were designed to be close to neutrally buoyant to minimize the external forcing on the vehicle. The majority of these vehicles were controlled through the use of fins and vectored thrust. With the introduction of the underwater glider, internal actuation took a more present role as a control method. By evaluating different methods of depth control for a positively buoyant vehicle, we will identify and choose the most energy efficient and effective method of control that does not violate the recovery requirement. Upon picking the control method, a module is designed and constructed to expand the low-speed functionality of the VTMAUV.

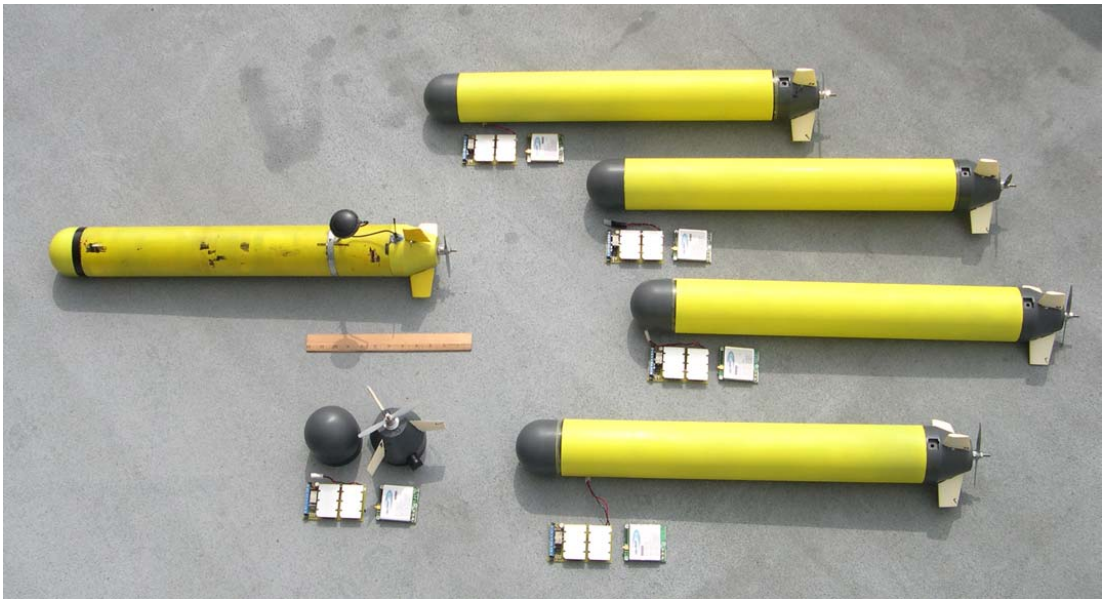

Figure 1.3: Fleet of VTMAUVs
Photo courtesy: Dr. Daniel Stilwell.

Chapter 2

Alternative Attitude Control Methods

To maintain a constant depth, a positively buoyant AUV must generate a continuous downward force at all times. This force is produced through either direct vertical thrust or through downward lift. Sections 2.1 and 2.2 will examine two methods of creating direct external forces for use of attitude and position control, while the remaining sections will focus on methods of internal actuation that provide control forces or control moments.

2.1 Vectored Thrusting

The easiest method of attitude control is to vector the thrust. This is accomplished though a mechanical redirection of the induced fluid flow from the jet nozzle or propeller or through a secondary set of vertically mounted thrusters. These thrusters are placed to give direct control authority in the body vertical direction. This method requires a constant fluid flow field where the effectiveness of the propulsor is scaled by the difference in the ambient fluid velocity and the core velocity of the accelerated fluid material. Because the craft is positively buoyant a constant opposing force must be maintained to keep depth. This constant force needs constant power, resulting in a continuous drain on the battery. This limits the mission duration. Additionally, this artificial flow field may interfere with the inspection mission by disturbing silt or aerating the water reducing visibility. More directly this flow field may undesirably interact with the object that the AUV is trying to inspect. AUVs like the previously mentioned ABE utilized this method for the added maneuverability benefits when working in rough terrain or around sunken vessels.

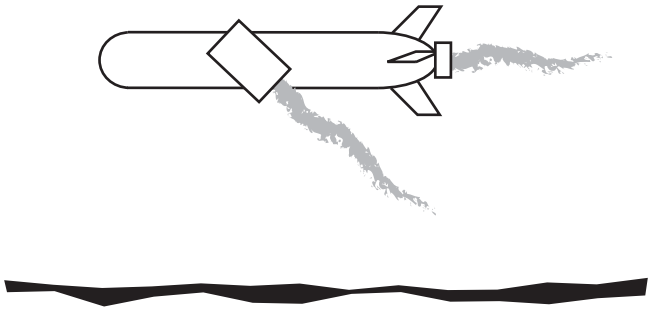

Figure 2.1: Vectored thrust

2.2 Biomimetic Thrusters

Another method of producing a direct force on the AUV uses movement of the fins, mimicking swimming aquatic life. In 1993, an oscillating foil was suggested as a method of propulsion [19]. Later work focused on control using fin movement devices [20]. This work led to the development of Draper Laboratory's RoboTuna [21]. Draper Laboratory uses this robotic tuna as a test platform for research in vortex manipulation of the eddies formed from this method of propulsion.

A disadvantage to this system of thrust is the impulse nature of the applied force. Forces created in this manner can fatigue mechanical structures and send vortical waves into the environment. These pressure waves can disturb the object under inspection, or if near a surface, can stir up sediment or aerate water reducing visibility. Because of the mechanical complexity necessary to simulate the bend of fish fin, this device is also more likely to fail. Finally, continuous power must be applied where a constant force is required, creating additional drain on the battery under positively buoyant conditions.

2.3 Reaction Wheels/Control Moment Gyros

By moving the control method inside the vehicle, one loses the ability to directly push on the fluid material. To counteract the vehicle buoyancy one must utilize the hydrodynamic properties of the wing-body. An angle of attack must be maintained to generate the necessary force to keep depth. This places emphasis on angular control up to the stall angle of the AUV.

The first method of internal actuation uses a rotor of significant rotational inertia that is spun up creating a reaction moment proportional to the acceleration of the rotating mass. These types of actuators are used as a primary rotational control method on spacecraft

and can be used to stabilize vehicle motions in underwater vehicles [22]. If fixed in the

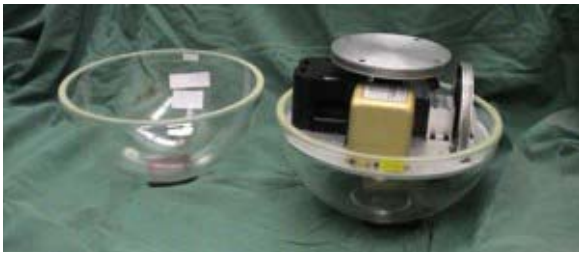

Figure 2.2: IAMBUS: Internally Actuated Modular Bodied Untethered Submersible

craft geometry to allow rotation about only one axis the actuator is known as a Reaction or Momentum Wheel. Allowing a rotation about an axis perpendicular to the axis of spin allows gyroscopic effects to be utilized. These devices are referred to as Control Moment Gyros (CMG). These gyroscopic effects generate an out of plane moment increasing the redundancy of a multiple CMG system [23]. Also once the top speed is reached, the actuator becomes saturated, no longer able to maintain a torque. Again like the external methods of actuation, this also requires a constant acceleration to generate a constant torque. It drains the battery stunting the mission lifetime of the vehicle.

2.4 Buoyancy Engine

A more energy conservative approach to actuator design is to use native environmental acceleration to create the force or moment needed to maintain depth or orientation. By displacing additional fluid through inflatable appendages a modification of the buoyancy force center and magnitude can be implemented. Alternatively, fluid material can be taken into the vehicle producing a variable point mass at a fixed location. This type of device, referred to as a ballast actuator, takes ballast from the surrounding medium to utilize the native material and gravitational field to impart the desired force or moment. The advantage to this technique lies in the energy cost of use per unit of continuous force or torque. This creates a very energy efficient actuator. This type of actuator is used by underwater gliders as a method of glide control and propulsion and a similar device is included in deep submersibles to maintain neutral buoyancy through small changes in fluid density. It should be noted that there are inherent dangers associated with bring an electrolytic fluid into an electronic filled body, however, through the used of careful design this fear can often be alleviated. This method of attitude control changes the buoyancy percentage. This change can violate the positive buoyancy requirement which was imposed so that the vehicle was recoverable in the event of a failure.

2.5 Moving Mass

One final method uses the idea of modifying the center or gravity by moving a percentage of the body weight forward or aft for pitch, port or starboard for roll. Moving a section of mass allows constant torque generation for a given energy input and is independent of the vehicle velocity. It is isolated from the outside environment resulting in no losses in efficiency from biological fouling, corrosion, and snagging. The actuator is mechanically simple, remains energy efficient, and the outside fluid remains undisturbed. The buoyancy percentage remains unmodified, requiring an increase in the body angle of attack to supplement the body lift at low speed. The moment necessary for this maneuver drives the mass sizing and the distance moved. This method provides the best constant torque per unit of control energy without violating the positively buoyant nature of the AUV. Development of a moving mass actuator is investigated in chapters 4 and 6.

Chapter 3

Force and Moment Modelling

In order to mathematically model and simulate a vehicle and its dynamic response, the vehicle forces and moments must first be modelled. Gravitational and hydrostatic constants depend on the vehicle density, fluid density, and displaced volume. The hydrodynamic constants are scaled from nondimensional empirical data through use of a reference area and length for similar shapes. The thruster is assumed throttled with a maximum thrust equal to at least the difference in buoyant and weight forces. Proper sizing is examined in the following chapter.

3.1 Coordinate Frames

A sign convention is first established by defining the vehicle coordinate frames and rotation angles (Fig. 3.1). Three reference frames are used to describe the motion of the vehicle. The body reference frame is centered on the geometric center (GEO) of the slender axisymmetric hull with the x_b axis running the longitudinal axis of symmetry. The body vertical component z_b, is defined normal to x_b in the plane containing the CG. This coordinate system is used to locate all body fixed locations as well as the moving mass position. To remain orthonormal y_b is defined out the starboard side of the AUV. We assume planar motion in the longitudinal body x-z plane, equating the orthonormal y_b axis with the Newtonian and velocity y axes.

We define the Newtonian/inertial reference frame by placing z_n along the gravitational vector and aligning the y_n vector with y_b. By assuming this is Newtonian, we neglect Coriolis acceleration from the earth's rotation. This is possible because this acceleration is much smaller in magnitude when compared to the gravitational acceleration.

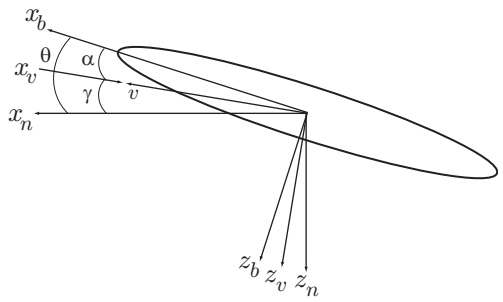

Figure 3.1: Reference frame orientation for subsequent calculations

The velocity reference frame is defined by placing the x_v axis along the vehicle velocity vector and aligning the y_v vector with y_b. For motions in the longitudinal plane, the body and Newtonian reference frames are related through a rotation about the common y axis through the angle θ, the body and velocity frames though the angle of attack (AoA) α, and the velocity to newtonian through the glide angle γ. Because all of these angles are measured about the same y-axis, they are related by:

$$\theta = \gamma + \alpha$$

Now that a system of coordinates has been defined, it is necessary to identify the reference areas and lengths in order to scale the empirical hydrodynamic data.

3.2 Geometrical Definitions

General areas and lengths used in the subsequent calculations of this paper follow those provided in Figure 3.2. The vehicle is assumed a cylindrical slender body of $\frac{L}{r} > 10$. The areas are defined as in the picture, where A_r is the reference area for which the hydrodynamic coefficients are dimensionalized, A_{ht} is the horizontal tail area, and A_p is the vehicle planform area. The body length, L, is used for the reference length. The length variables x_c, x_m, and x_{ac} are the vehicle half length, moment reference location, and aerodynamic center respectively. The wing, when included, is assumed to be placed such that the aerodynamic center (AC) of the wing-body is at the half length at low velocity. This is done to minimize the velocity dependent travel of the AC as well as to minimize the associated moment.

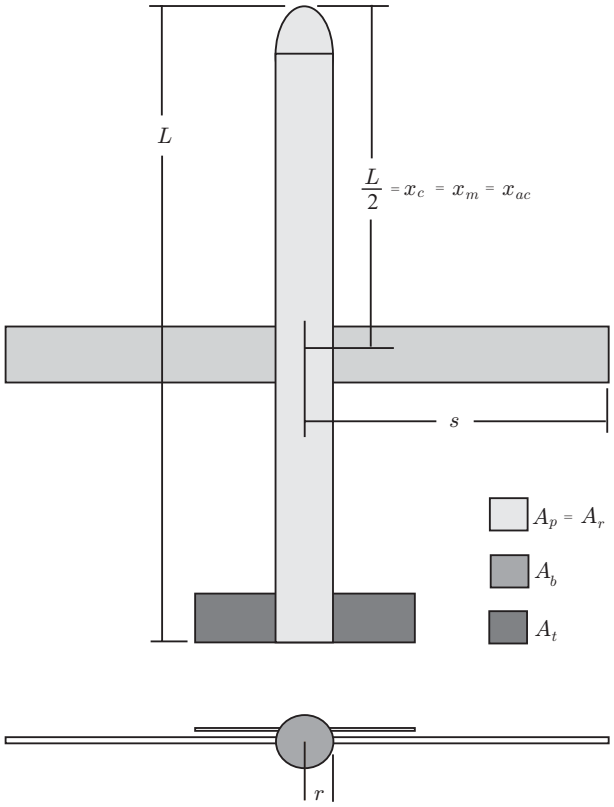

Figure 3.2: Reference lengths and areas

3.3 Example Vehicle

In the subsequent calculations it is necessary to define a first iteration of the vehicle physical constants. The characteristics of the Virginia Tech Miniature Autonomous Underwater Vehicle (VTMAUV) (Fig. 3.3) provide this starting point from which the wing span and buoyancy factors can be iterated to examine their effect. The values used are:

Characteristic	Value
r	1.875 in
$\frac{L}{r}$	15.5
$\frac{s}{r}$	1 (No Wings)
$\frac{B}{W}$	1.02

In the proper range, the effect of these iterated constants will maximize the depth control efficiency of the AUV, minimizing the expended energy or maximizing the lowest achievable velocity. However, before this can be done the forces and moments must first

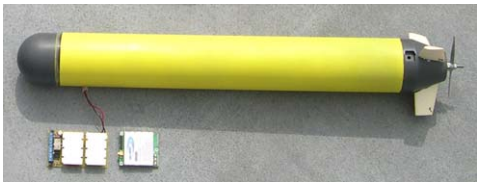

Figure 3.3: Virginia Tech Miniature Autonomous Underwater Vehicle (VTMAUV)

be correctly defined.

3.4 Forces and Moments

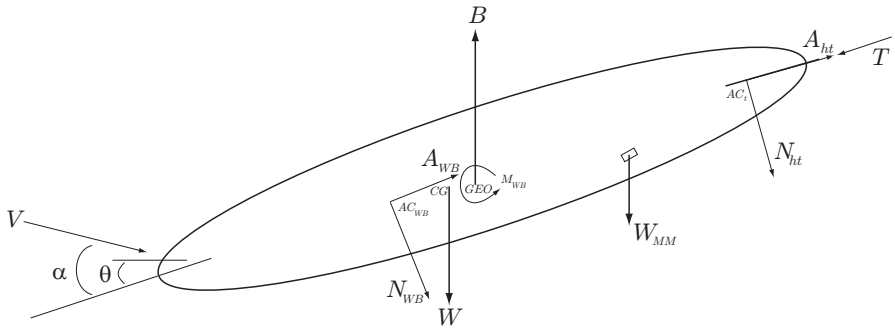

Figure 3.4: Force diagram for a conventional streamlined AUV

Now that we have identified the reference areas and lengths we begin to model the vehicle forcing. Figure 3.4 shows a basic force diagram displaying the forces and their force centers. The center of buoyancy is assumed at the vehicle geometric center, which is generally an accurate assumption for a pressured axisymmetric hull. The center of gravity is assumed to be offset from the center of buoyancy creating a constant gravitational torque defined by:

$$\boldsymbol{M}_{cg} = \boldsymbol{r}_{cg} \times \boldsymbol{W} = \begin{bmatrix} r_{cg_x} \\ 0 \\ r_{cg_z} \end{bmatrix} \times \begin{bmatrix} 0 \\ 0 \\ mg \end{bmatrix} = -mgr_{cg_x}\vec{\boldsymbol{j}}_b$$

Here $\boldsymbol{r}_{cg}$ is defined as the distance between the center of gravity and the center of buoyancy (CB) with components r_{cg_x}, r_{cg_y}, r_{cg_z} in the body frame. This gravitational torque is the only force that is not directly dependent on the vehicle velocity.

Also effective at low speed is the vehicle thruster. The thrust produced from the propulsor is proportional to the velocity difference between the vehicle speed and the speed of the

thrust slipstream. This Δv correlates to the change in pressure per unit area created by the propeller or jet.

The last and most important force group is the hydrodynamics. This group is composed of the N_{wb}, A_{wb}, N_{ht}, and A_{ht} forces which act normal and axial to the hydrodynamic surface. These are related to the longitudinal axis through the angle θ. Understanding these forces and moments is necessary for predicting the failure speed, which occurs when the vehicle can no longer counteract the positive net buoyancy of the craft. These forces are affected by area and placement.

3.4.1 Wing-body Hydrodynamics

We begin by defining the following normal-force and pitching-moment coefficients as taken from [24] for a slender body with a constant shape over its length:

$$C_{N_{wb}} = \frac{A_b}{A_r} \sin 2\alpha \cos\frac{\alpha}{2} \left(\frac{C_N}{C_{N_0}}\right)_{SB} + \eta C_{d_n} \frac{A_p}{A_r} \sin^2\alpha \left(\frac{C_N}{C_{N_0}}\right)_{Newt} \tag{3.1}$$

$$C_{A_{wb}} = C_{A_{wb_0}} \cos^2\alpha \tag{3.2}$$

$$\begin{aligned} C_{m_{wb}} \quad = \quad & \left\{\left[\frac{\nabla - A_b(L - x_m)}{A_r X}\right] \sin 2\alpha \cos\frac{\alpha}{2}\right\} \left(\frac{C_m}{C_{m_0}}\right)_{SB} \\ & + \left[\eta C_{d_n} \frac{A_p}{A_r} \left(\frac{x_m - x_c}{X}\right) \sin^2\alpha\right] \left(\frac{C_m}{C_{m_0}}\right)_{Newt} \end{aligned} \tag{3.3}$$

where

$$\left(\frac{C_N}{C_{N_0}}\right)_{SB} = \left(\frac{C_m}{C_{m_0}}\right)_{SB} = \left(\frac{s}{r}\right)^2 + \left(\frac{r}{s}\right)^2 - 1 \tag{3.4}$$

and

$$\left(\frac{C_N}{C_{N_0}}\right)_{Newt} = \left(\frac{C_m}{C_{m_0}}\right)_{Newt} = \frac{3}{2}\left(\frac{s}{r} - \frac{1}{3}\right) \tag{3.5}$$

Equation 3.3 shows the wing-body destabilizing pitching moment. This hydrodynamic destabilizing moment varies quadratically with velocity and is offset with a properly sized horizontal tail. A component of the body lifting force, $C_{N_{wb}}$, along with the component of thrust in the z_n direction is responsible for maintaining depth. This lifting force is maximized though an increase in the wing span, s. The first terms in equations 3.1 and 3.3 represent the contribution from slender-body theory. This is followed by a correction in the second set of terms for the viscous crossflow and flow separation effects. Terms

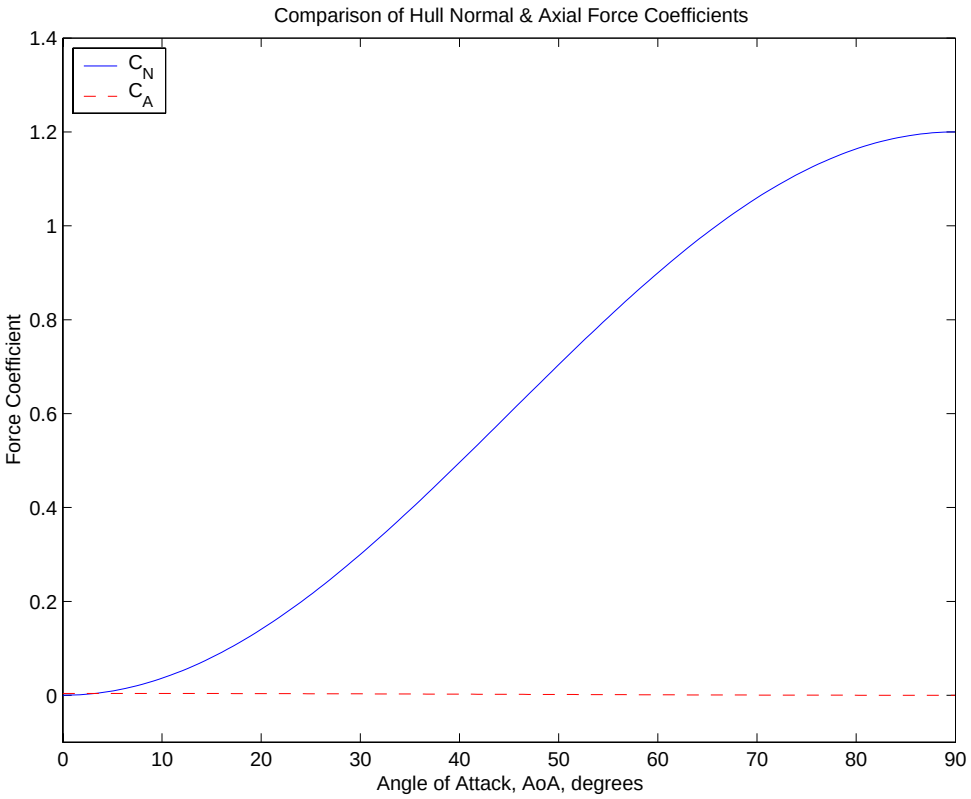

Figure 3.5: Comparison of normal and axial hull force coefficients

denoted with the subscript SB are determined from slender-theory and subsequently subscripts of $Newt$ are determined from Newtonian theory. The relations stated in 3.4 and 3.5 are valid as long as the cross-sectional shape is constant over the hull length.

The term C_{d_n} is the crossflow drag coefficient for a 2-D circular cylinder normal to an airstream. For a circular cross section, C_{d_n} is found to be approximately 1.20. Using this information with the lengths and areas defined in section 3.2, the vehicle wing-body forcing is plotted in figure 3.5. This figure shows the relative magnitudes of the normal and axial hull force coefficients. This graph is dominated by the normal force coefficient and when the vehicle is inclined the component of the normal force in the z_n is much larger than the component of the axial force in the same direction. This allows the axial force coefficient to be neglected when the two are compared.

3.4.2 Fin Hydrodynamics

The effect of the horizontal tail plays a role in the overall net hydrodynamic lifting force on the vehicle. This term scales linearly with the ratio of areas, $\frac{A_t}{A_r}$, resulting in:

$$C_N = C_{N_{wb}} + \frac{A_t}{A_r} C_{N_{ht}}$$

The equations for $C_{N_{ht}}$ and $C_{A_{ht}}$ are taken from [25] and apply to a two dimensional flat plate that has been adjusted to fit empirical data.

$$C_{N_{ht}} = \frac{1}{0.222 + \frac{0.283}{\sin \alpha}} \tag{3.6}$$

and

$$C_{A_{ht}} = C_{D_{f_0}} \cos^2 \alpha_f \tag{3.7}$$

The vertical tail force coefficients $C_{N_{vt}}$ and $C_{A_{vt}}$ are defined as:

$$C_{N_{vt}} = \frac{1}{0.222 + \frac{0.283}{\sin \beta}} \tag{3.8}$$

and

$$C_{A_{vt}} = C_{D_{f_0}} \cos^2 \beta \tag{3.9}$$

The term $C_{D_{f_0}}$ is the overall net drag coefficient for a straight and level zero deflection condition. A comparison of the fin normal and axial forces shown in Figure 3.6 displays the same dominance of the normal force coefficient over the axial coefficient as with the wing-body. Using these force coefficient models, the horizontal tail is sized as later discussed in section 5.2.

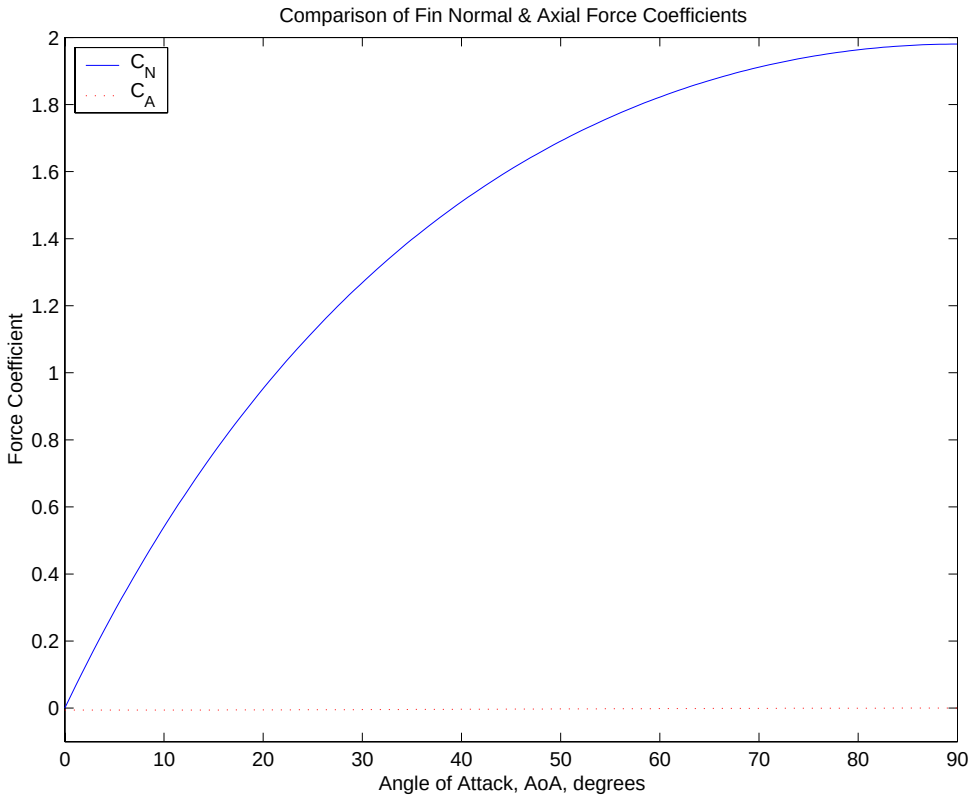

Figure 3.6: Comparison of normal and axial fin force coefficients

Chapter 4

Moving Mass

In the presence of a gravitational field, movement of an internal mass changes the location of the system's center of gravity. This movement creates a gravitational torque on the body with a magnitude proportional to the amount of mass moved and the distance it was moved. The moving mass effect can also induce undesirable dynamics through fuel sloshing [26]. By understanding this effect an energy efficient controller can be developed for use on an AUV. This chapter will develop the full seven degree of freedom (DOF) model and restrict movement to longitudinal motion (four DOF) to be later used to evaluate the depth control ability of the wing-body and moving mass combination.

4.1 Kinematics

Before the dynamics of the moving mass wing-body system can be fully developed the vehicle's kinematic model must first be defined. The kinematic model is a description of the movement of the vehicle geometry. This model is described through a progression of rotations about different axes. This progression is used to build a rotation matrix which transforms a vector from one reference frame to another. This rotation matrix $\boldsymbol{R}$ can be developed by several different methods, each with advantages and disadvantages. A common method of building this matrix uses three consecutive rotations, denoted as Euler angles, about a progression of axes. The order in which these rotations occur determines the ending location in three space. Euler angles give a more physical picture of the vehicle attitude at small angles, which is why they are more often used than alternative construction methods like quaternions or direction cosines.

We begin by defining the inertial position vector as $\boldsymbol{b} = [x\ y\ z]^T$, the body velocity

vector as $\boldsymbol{v} = [u\ v\ w]^T$, and the body angular velocity vector as $\boldsymbol{\Omega} = [p\ q\ r]^T$. This transformation is completed though a rotation about the angles $\boldsymbol{\Phi} = [\theta_x\ \theta_y\ \theta_z]^T$ so that the 3-2-1 rotation matrix from the body to newtonian reference frame becomes:

$$\boldsymbol{R} = \begin{bmatrix} \cos\theta_y \cos\theta_z & \sin\theta_x \sin\theta_y \cos\theta_z - \cos\theta_x \sin\theta_z & \cos\theta_x \sin\theta_y \cos\theta_z + \sin\theta_x \sin\theta_z \\ \cos\theta_y \sin\theta_z & \sin\theta_x \sin\theta_y \sin\theta_z + \cos\theta_x \cos\theta_z & \cos\theta_x \sin\theta_y \sin\theta_z - \sin\theta_x \cos\theta_z \\ -\sin\theta_y & \sin\theta_x \cos\theta_y & \cos\theta_x \cos\theta_y \end{bmatrix} \tag{4.1}$$

For a straight and level initial condition this rotation matrix simplifies to:

$$\boldsymbol{R}_0 = \boldsymbol{I}_{3\times 3}$$

The inverse of this rotation matrix is equal to its transpose. For the purpose of simplification we define the $\hat{\cdot}$ operator to convert a vector into a skew-symmetric matrix so that:

$$\boldsymbol{a} \times \boldsymbol{b} = \hat{\boldsymbol{a}}\boldsymbol{b} = \begin{bmatrix} 0 & -a_x & a_y \\ a_x & 0 & -a_z \\ -a_y & a_z & 0 \end{bmatrix} \begin{pmatrix} b_x \\ b_y \\ b_z \end{pmatrix}$$

Using this notation, a description of the attitude kinematics is:

$$\dot{\boldsymbol{R}} = \boldsymbol{R}\hat{\boldsymbol{\Omega}} \tag{4.2}$$

The angular rate expression becomes:

$$\begin{pmatrix} \dot{\theta_x} \\ \dot{\theta_x} \\ \dot{\theta_x} \end{pmatrix} = \begin{bmatrix} 1 & \sin\theta_x \tan\theta_y & \cos\theta_x \tan\theta_y \\ 0 & \cos\theta_x & -\sin\theta_x \\ 0 & \sin\theta_z \sec\theta_y & \cos\theta_x \sec\theta_y \end{bmatrix} \begin{pmatrix} p \\ q \\ r \end{pmatrix}$$

This matrix has a singularity at $\theta_y = \pm 90°$ but works well for the range of pitch angles

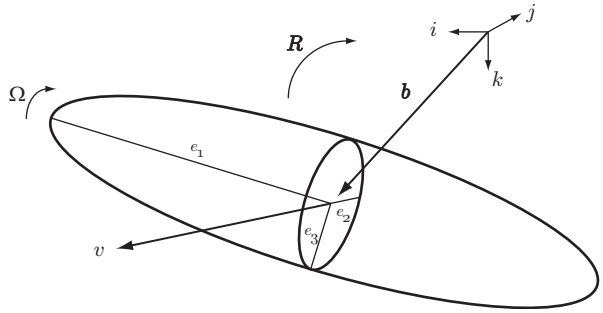

Figure 4.1: Position and orientation variables

below the stall angle of the wing-body. The inertial velocity of the vehicle takes the form:

$$\dot{\boldsymbol{b}} = \boldsymbol{R}\boldsymbol{v} \tag{4.3}$$

The inertial velocity of the point mass m_p becomes:

$$\boldsymbol{v}_p = \boldsymbol{R}\,\dot{\boldsymbol{r}}_p$$

where $\boldsymbol{r}_p$ is the vector that describes the body-relative position of the moving mass. Restricting this movement to act only along the body longitudinal axis, creates the following vector:

$$\dot{\boldsymbol{r}}_p = r_p\vec{\boldsymbol{e}_1} = \begin{pmatrix} \dot{r_p} \\ 0 \\ 0 \end{pmatrix} \tag{4.4}$$

Here the vector $\vec{\boldsymbol{e}_1}$ is defined as the first column of the identity matrix.

$$\boldsymbol{I}_{3\times3} = \begin{bmatrix} \vec{\boldsymbol{e}}_1 & \vec{\boldsymbol{e}}_2 & \vec{\boldsymbol{e}}_3 \end{bmatrix} = \begin{bmatrix} 1 & 0 & 0 \\ 0 & 1 & 0 \\ 0 & 0 & 1 \end{bmatrix}$$

Now that we have a method of describing the motion of the vehicle we can begin to evaluate the forced dynamics of the AUV and moving mass.

4.2 Dynamics

We define our state vector as a combination of the vehicle angular momentum $\boldsymbol{\Pi}$, the vehicle linear momentum $\boldsymbol{P}$, and the linear momentum of the point mass P_p $\left(\boldsymbol{s} = [\boldsymbol{\Pi}^T\ \boldsymbol{P}^T\ P_p^T]^T\right)$. Combining the linear and angular velocity vectors with the moving mass velocity $\dot{\boldsymbol{r}}_p$ forms $\bar{v} = [\boldsymbol{\Omega}^T\ \boldsymbol{v}^T\ \dot{\boldsymbol{r}}_p^T]^T$. These terms are related through:

$$\boldsymbol{s} = \boldsymbol{I}\bar{\boldsymbol{v}}$$

Rearranging this equation, the angular, linear, and moving mass velocities are found.

$$\bar{\boldsymbol{v}} = \boldsymbol{I}^{-1}\boldsymbol{s}$$

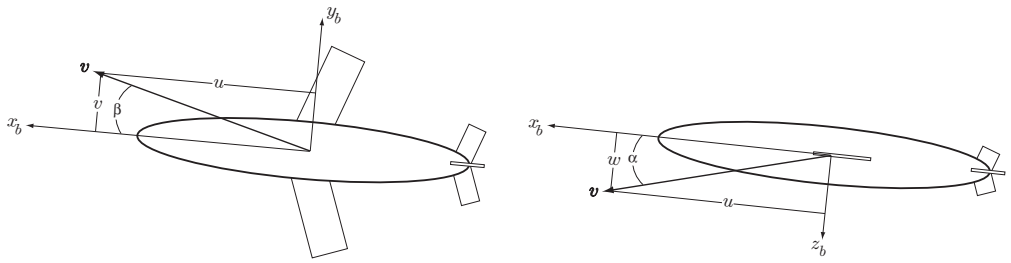

Figure 4.2: The hydrodynamic angles

Using the body translation velocities, $\boldsymbol{v} = (u\ v\ w)^T$, the hydrodynamic angles are identified (figure 4.2). The angle of attack is defined as:

$$\alpha = \tan^{-1}\left(\frac{w}{u}\right)$$

The sideslip angle is defined as:

$$\beta = \tan^{-1}\left(\frac{v}{u}\right)$$

These two angles define our hydrodynamic velocity reference frame which are used in conjunction with conventional lift and drag coefficients. It should be noted that because we are evaluating the x-z planar pitch case, β should be zero as a result of a zero side velocity v.

Using these angles, we recall the hydrodynamic modelling from sections 3.4.1 and 3.4.2 and are able to assemble the hydrodynamic forcing in the body frame.

$$\boldsymbol{F}_{Hydro} = \begin{pmatrix} -A_{wb} - \frac{A_t}{A_r}A_{ht} \\ 0 \\ -N_{wb} - \frac{A_t}{A_r}N_{ht} \end{pmatrix} \tag{4.5}$$

The remaining hydrostatic and gravitational external forces are rotated to the body frame using the transpose of the rotation matrix from equation 4.1. We assume the propulsor is fixed in the AUV and aligned on the centerline at the rear of the vehicle. Grouping these forces together yields:

$$\boldsymbol{F}_{grav} = (m_b + m_p - m_{buoy})g\boldsymbol{R}^T\vec{\boldsymbol{e}_3} \tag{4.6}$$

The total external forcing on the vehicle is therefore a combination of equations 4.5, 4.6, and the body thrust.

$$\boldsymbol{f}_{ext} = \boldsymbol{F}_{aero} + \boldsymbol{F}_{grav} + T\vec{\boldsymbol{e}_1} \tag{4.7}$$

The external moments acting on the AUV are broken down in the following manner:

$$\Sigma\boldsymbol{M}_{ext} = \boldsymbol{M}_{wb} + \boldsymbol{M}_{ht} + \boldsymbol{M}_{vt} + \boldsymbol{M}_{cg} + \boldsymbol{M}_p$$

The wing-body moment $\boldsymbol{M}_{wb}$ is taken about x_b and is defined in section 3.4.1. It is derived from slender-body theory and corrected to account for viscous crossflow. The terms $\boldsymbol{M}_{ht}$ and $\boldsymbol{M}_{vt}$ account for the moments caused by the horizontal and vertical tails and are defined as:

$$\boldsymbol{M}_{ht} = \hat{\boldsymbol{r}}_{ht} \times \begin{pmatrix} C_{A_{ht}} \\ 0 \\ C_{N_{ht}} \end{pmatrix}, \quad \boldsymbol{M}_{vt} = \hat{\boldsymbol{r}}_{vt} \times \begin{pmatrix} C_{A_{vt}} \\ 0 \\ C_{N_{vt}} \end{pmatrix}$$

The terms $C_{N_{ht}}$, $C_{N_{vt}}$, $C_{A_{ht}}$, and $C_{A_{vt}}$ are defined in section 3.4.2. The moment due to an offset CG is:

$$\boldsymbol{M}_{cg} = \hat{\boldsymbol{r}}_{cg} \times \begin{pmatrix} 0 \\ 0 \\ m_b g \end{pmatrix}$$

This moment is the AUV CG offset without influence from the moving mass actuator. The moment of the moving mass is treated separately and is defined as:

$$\boldsymbol{M}_{p} = \hat{\boldsymbol{r}}_{p} \times \begin{pmatrix} 0 \\ 0 \\ m_p g \end{pmatrix}$$

The thruster is assumed to produce a thrust vector that passes through the point of rotation. This eliminates any contributions to moment generation from the fixed thruster. It should be noted that when using a propeller, there is a roll moment equal and opposite to the moment exerted on the fluid to add vorticity. We ignore this small effect; a sufficiently low CG will counter the roll moment due to thrust.

With these models of the external force and moments, the forced equations of motion can be derived. However, before these are developed, it is necessary to accurately model the moments of inertia as they vary with the moving mass position.

4.2.1 Inertia

The primary function of the moving mass is to act as a rotational control device. For this reason, the rotational dynamics are of first concern, governed and modified though the torques on the body. To understand these motions, the mass distribution of the craft must be evaluated to develop the mass moments of inertia to be used in Newton's equations of rotational motion. The inertia tensor is computed in the body frame for convenience. This body inertia tensor is defined by the vehicle's cylindrical shape. (The

vehicle density is assumed constant.)

$$\begin{aligned} \boldsymbol{I}_b &= \begin{bmatrix} \frac{1}{2}m_b r^2 & 0 & 0 \\ 0 & \frac{1}{12}m_b L^2 + \frac{1}{4}m_b r^2 & 0 \\ 0 & 0 & \frac{1}{12}m_b L^2 + \frac{1}{4}m_b r^2 \end{bmatrix} \\ &= m_b r^2 \begin{bmatrix} \frac{1}{2} & 0 & 0 \\ 0 & \frac{1}{12}\left(\frac{L}{r}\right)^2 + \frac{1}{4} & 0 \\ 0 & 0 & \frac{1}{12}\left(\frac{L}{r}\right)^2 + \frac{1}{4} \end{bmatrix} \end{aligned}$$

This moment of inertia works well for a constant density shape where the center of gravity matches the geometric center. This however is not often the case, resulting in a correction due to the generalized inertia of the offset CG.

$$\boldsymbol{I}_{cg} = \begin{bmatrix} \mathbf{0}_{3\times3} & m_b\hat{\boldsymbol{r}}_{cg} & \mathbf{0}_{3\times1} \\ -m_b\hat{\boldsymbol{r}}_{cg} & m_b\boldsymbol{I}_{3\times3} & \mathbf{0}_{3\times1} \\ \mathbf{0}_{1\times3} & \mathbf{0}_{1\times3} & 0 \end{bmatrix} \tag{4.8}$$

The moving point mass affects the rotational inertia as well, resulting in:

$$\boldsymbol{I}_p = \begin{bmatrix} \mathbf{0}_{3\times3} & m_p\hat{\boldsymbol{r}}_p & m_p\hat{\boldsymbol{r}}_p\vec{\boldsymbol{e}}_1 \\ -m_p\hat{\boldsymbol{r}}_p & m_p\boldsymbol{I}_{3\times3} & m_p\vec{\boldsymbol{e}}_1 \\ -m_p\vec{\boldsymbol{e}}_1^{\,T}\hat{\boldsymbol{r}}_p & m_p\vec{\boldsymbol{e}}_1^{\,T} & m_p \end{bmatrix} \tag{4.9}$$

Combining these terms, the new 7×7 matrix is:

$$\boldsymbol{I}_{system} = \begin{bmatrix} \boldsymbol{I}_b - m_p\hat{\boldsymbol{r}}_p\hat{\boldsymbol{r}}_p & m_b\hat{\boldsymbol{r}}_{cg} + m_p\hat{\boldsymbol{r}}_p & m_p\hat{\boldsymbol{r}}_p\vec{\boldsymbol{e}}_1 \\ -m_b\hat{\boldsymbol{r}}_{cg} - m_p\hat{\boldsymbol{r}}_p & (m_b + m_p)\boldsymbol{I}_{3\times3} & m_p\vec{\boldsymbol{e}}_1 \\ -m_p\vec{\boldsymbol{e}}_1^{\,T}\hat{\boldsymbol{r}}_p & m_p\vec{\boldsymbol{e}}_1^{\,T} & m_p \end{bmatrix} \tag{4.10}$$

4.2.2 Added Mass and Inertia

When moving, a vehicle must force its way through the fluid medium. The effect of moving this fluid material around the craft imparts a force that opposes the acceleration. Because of the way that this force behaves, mass and inertia are added to the vehicle model to produce the equivalent effect. This added mass and inertia depend on the AUV shape and the fluid density. For a slender axisymmetric vehicle hull, this added mass and inertia are diagonal and follow the sign convection of standard SNAME notation [27].

$$\boldsymbol{I}_f = -diag\left\{\boldsymbol{J}_f, \boldsymbol{M}_f\right\} = -diag\left\{K_{\dot{p}}, M_{\dot{q}}, N_{\dot{r}}, X_{\dot{u}}, Y_{\dot{v}}, Z_{\dot{w}}\right\}$$

Models for added mass and inertia vary with the three dimensional shape of the vehicle. One of the easiest shapes to model is a spheroid. Using the information from [25] the cylindrical volume is matched to its ellipsoidal equivalent and used as an approximation to the true axisymmetric hull.

The volume of an ellipsoid is defined as:

$$\forall_e = \frac{4}{3}abc$$

where a, b, and c are lengths defined in figure 4.3. Here $b = c = r$ resulting in:

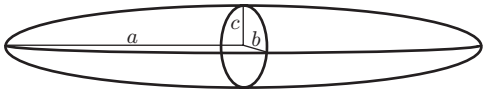

Figure 4.3: Length dimensions for a axisymetric spheroidal volume

$$\forall_e = \frac{4}{3}\pi a r^2 \tag{4.11}$$

This volume is matched to the volume of the cylindrical hull defined by:

$$\forall_c = \pi r^2 L \tag{4.12}$$

where r and L are defined in figure 4.4.

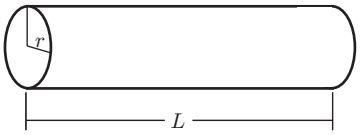

Figure 4.4: Length dimensions for a cylindrical volume

Equating equations 4.11 and 4.12 it is found that for equivalent volumes the length a of the spheroid must follow:

$$a = \frac{3}{4}L \tag{4.13}$$

This results in a vehicle that is 1.5 times the original length but encompasses the effect of the rounded nose and tapered tail sections.

Using this relation the following constants can be calculated.

$$e = \sqrt{1 - \left(\frac{b}{a}\right)^2}$$

$$\alpha_0 = \frac{2\left(1-e^2\right)}{e^3}\left(\frac{1}{2}\ln\frac{1+e}{1-e} - e\right)$$

$$\beta_0 = \frac{1}{e^2} - \frac{1-e^2}{2e^3}\ln\frac{1+e}{1-e}$$

Using these we define:

$$k_1 = \frac{\alpha_0}{2-\alpha_0}$$

$$k_2 = \frac{\beta_0}{2-\beta_0}$$

$$k' = \frac{e^4\left(\beta_0 - \alpha_0\right)}{\left(2-e^2\right)\left[2e^2 - \left(2-e^2\right)\left(\beta_0 - \alpha_0\right)\right]}$$

These k-values are used to calculate the diagonal elements of the added mass and inertia matrix.

$$\begin{aligned} X_{\dot{u}} &= -k_1 m \\ Y_{\dot{v}} = Z_{\dot{w}} &= -k_2 m \\ N_{\dot{r}} = M_{\dot{q}} &= -k' I_y \\ K_{\dot{p}} &= 0 \end{aligned}$$

Combining the wing-body with the fluid inertia yields the system total inertia about the vehicle geometric center.

$$\boldsymbol{I} = \boldsymbol{I}_{system} + \boldsymbol{I}_f = \begin{bmatrix} \boldsymbol{I}_b - m_p\hat{\boldsymbol{r}}_p\hat{\boldsymbol{r}}_p + \boldsymbol{J}_f & m_b\hat{\boldsymbol{r}}_{cg} + m_p\hat{\boldsymbol{r}}_p & m_p\hat{\boldsymbol{r}}_p\vec{\boldsymbol{e}}_1 \\ -m_b\hat{\boldsymbol{r}}_{cg} - m_p\hat{\boldsymbol{r}}_p & (m_b+m_p)\boldsymbol{I}_{3\times3} + \boldsymbol{M}_f & m_p\vec{\boldsymbol{e}}_1 \\ -m_p\vec{\boldsymbol{e}}_1{}^T\hat{\boldsymbol{r}}_p & m_p\vec{\boldsymbol{e}}_1{}^T & m_p \end{bmatrix} \tag{4.14}$$

With this inertia matrix as a function of the moving mass position, we can evaluate the equations of motion of the AUV-moving mass system.

4.3 Equations of Motion

The equations of motion are derived by computing the momenta of the vehicle-fluid system and applying Newton's laws. We define $\boldsymbol{p}$ as the total translational momentum of the vehicle-fluid system taken with respect to the inertial coordinate frame. Similarly, $\boldsymbol{\pi}$ is taken to represent the total angular momentum about the inertial coordinate origin with respect to the inertial frame. $\boldsymbol{p_m}$ is taken as the total translational momentum of the movable point mass. Using these momenta Newton's laws state:

$$\begin{aligned} \dot{\boldsymbol{p}} &= \sum_{i=1}^{I} \boldsymbol{f_{ext_i}} \\ \dot{\boldsymbol{\pi}} &= \sum_{i=1}^{I} (\boldsymbol{x_i} \times \boldsymbol{f_{ext_i}}) + \sum_{j=1}^{J} \boldsymbol{m_{ext_j}} \\ \dot{\boldsymbol{p}}_{\boldsymbol{p}} &= m_p g \boldsymbol{k} + \sum_{k=1}^{K} \boldsymbol{f_{int}} \end{aligned} \tag{4.15}$$

Here $\boldsymbol{k}$ represents the unit vector that points in the direction of gravity. The term $\boldsymbol{f_{ext}}$ is the total external forcing applied to the system as depicted by equation 4.7. A pure external torque on the system is represented with the term $\boldsymbol{M_{ext}}$.

We now define $\boldsymbol{P}$ to be the translational momentum of the fluid-body system with respect to the body frame. Let $\boldsymbol{\Pi}$ represent the total angular momentum of the fluid-body system, and define $\boldsymbol{P_p}$ as the point mass momentum, all with respect to the body reference frame.

$$\begin{aligned} \boldsymbol{p} &= \boldsymbol{RP} \\ \boldsymbol{\pi} &= \boldsymbol{R\Pi} + \boldsymbol{b} \times \boldsymbol{p} \\ \boldsymbol{p_p} &= \boldsymbol{RP_p} \end{aligned} \tag{4.16}$$

Differentiating equations 4.16 and using the kinematic relations 4.2 and 4.3 yields:

$$\begin{aligned} \dot{\boldsymbol{p}} &= \boldsymbol{R}\left(\dot{\boldsymbol{P}} + \hat{\boldsymbol{\Omega}}\boldsymbol{P}\right) \\ \dot{\boldsymbol{\pi}} &= \boldsymbol{R}\left(\dot{\boldsymbol{\Pi}} + \hat{\boldsymbol{\Omega}}\boldsymbol{\Pi}\right) + \boldsymbol{Rv} \times \boldsymbol{p} + \boldsymbol{b} \times \dot{\boldsymbol{p}} \\ \dot{\boldsymbol{p}}_{\boldsymbol{p}} &= \boldsymbol{R}\left(\dot{\boldsymbol{P}}_{\boldsymbol{p}} + \hat{\boldsymbol{\Omega}}\boldsymbol{P_p}\right) \end{aligned} \tag{4.17}$$

Substituting the equations of 4.15 for the time derivatives of the inertial momentum allows the following set of equations in body coordinates:

$$\begin{aligned}
\dot{\boldsymbol{P}} &= \boldsymbol{P} \times \boldsymbol{\Omega} + \boldsymbol{R^T} \sum_{i=1}^{I} \boldsymbol{f_{ext_i}} \\
\dot{\boldsymbol{\Pi}} &= \boldsymbol{\Pi} \times \boldsymbol{\Omega} + \boldsymbol{P} \times \boldsymbol{v} + \boldsymbol{R^T} \sum_{i=1}^{I} ((\boldsymbol{x_i} - \boldsymbol{b}) \times \boldsymbol{f_{ext_i}}) + \boldsymbol{R^T} \sum_{j=1}^{J} \boldsymbol{m_{ext_j}} \\
\dot{\boldsymbol{P_p}} &= \boldsymbol{P_p} \times \boldsymbol{\Omega} + m_p g \boldsymbol{R^T k} + \boldsymbol{R^T} \sum_{k=1}^{K} \boldsymbol{f_{int}}
\end{aligned} \tag{4.18}$$

Using these equations we can effectively model the system and evaluate the static conditions necessary for depth regulation and low speed control.

Chapter 5

Hydrodynamic Sizing

Sizing of a streamlined AUV is a balance between payload integration, steady flight optimization, and the satisfaction of dynamic maneuverability requirements. This chapter will focus on the static analysis that goes behind the sizing of the hydrodynamic surfaces to optimize the vehicle for low speed depth regulation. Evaluation of the steady state equilibrium conditions presents a relation between the vehicle geometry and the low speed flight conditions.

5.1 Equilibrium

An equilibrium motion is a condition where the vehicle velocity is unchanging over time. Recalling the dynamic equations from Chapter 4.2 we set the time derivatives to zero.

$$\begin{aligned} \dot{\boldsymbol{P}} &= \mathbf{0} = \boldsymbol{P} \times \boldsymbol{\Omega} + \sum_{i=1}^{I} \boldsymbol{F_{ext_i}} \\ \dot{\boldsymbol{\Pi}} &= \mathbf{0} = \boldsymbol{\Pi} \times \boldsymbol{\Omega} + \boldsymbol{P} \times \boldsymbol{v} + \sum_{j=1}^{J} \boldsymbol{M_{ext_i}} \end{aligned}$$

For equilibrium in longitudinal flight, we define $\boldsymbol{\Omega} = [0\ 0\ 0]^T$ and $\boldsymbol{v} = [u\ 0\ w]^T$. Because the angular velocity vector is zero, the first terms in the previous equations vanish

resulting in:

$$\sum_{i=1}^{I} \boldsymbol{F_{ext_i}} = \mathbf{0} \tag{5.1}$$

$$\sum_{j=1}^{J} \boldsymbol{M_{ext_i}} = \boldsymbol{P} \times \boldsymbol{v} \tag{5.2}$$

These two equations represent the vector equilibrium motion conditions for the streamlined underwater vehicle.

5.1.1 Condition 1: $\Sigma F = 0$

We identify the forces and moments on the streamlined AUV as shown in figure 5.1. Equation 5.1 requires that the sum of forces in the body frame must be zero to maintain

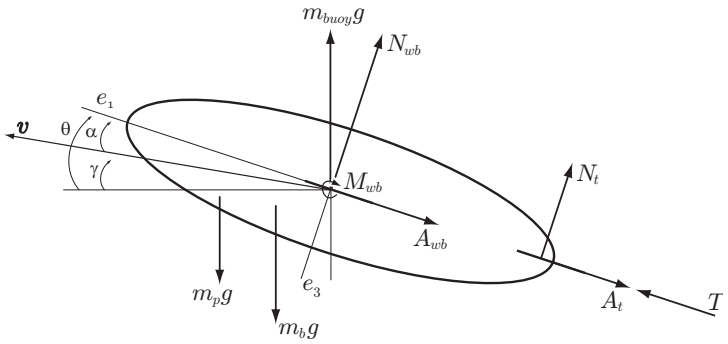

Figure 5.1: Force diagram for a streamlined AUV

this equilibrium set of states. Taking the summation of forces in the inertial z_n direction, we require $\dot{z} = 0$ for constant depth flight.

$$(m_b + m_p - m_{buoy})\, g = (N_{wb} + N_t)\cos\theta - (A_{wb} + A_t)\sin\theta + T\sin\theta \tag{5.3}$$

For simplicity we define:

$$\begin{aligned} m_T &= (m_b + m_p - m_{buoy}) \\ N_T &= (N_{wb} + N_t) \\ A_T &= (A_{wb} + A_t) \end{aligned}$$

which reduces equation 5.3 to:

$$m_T g = N_T \cos\theta - A_T \sin\theta + T\sin\theta \tag{5.4}$$

A summation of forces in the inertial x_n direction yields the necessary thrust condition. Using the constant velocity flight condition, $\dot{V} = \ddot{x} = 0$, the expression for thrust becomes:

$$\begin{aligned} 0 &= T\cos\theta - (A_{wb} + A_t)\cos\theta - (N_{wb} + N_t)\sin\theta \\ T &= (A_{wb} + A_t) + (N_{wb} + N_t)\tan\theta \end{aligned} \tag{5.5}$$

Inserting equation 5.5 into equation 5.3 yields:

$$\begin{aligned} m_T g &= N_T\cos\theta - A_T\sin\theta + A_T\sin\theta + N_T\tan\theta\sin\theta \\ &= N_T\cos\theta + N_T\tan\theta\sin\theta \\ &= N_T\cos\theta\left(1 + \tan^2\theta\right) \\ &= N_T\cos\theta\sec^2\theta \\ \Rightarrow N_T &= m_T g\cos\theta \\ \Rightarrow \bar{q} &= \frac{m_T g\cos\theta}{(C_{N_{wb}}A_r + C_{N_t}A_t)} \end{aligned} \tag{5.6}$$

Equation 5.6 relates the angle θ to the equilibrium velocity where we have used the fact that $\theta = \alpha$ for constant depth flight. Defining the dynamic pressure as: $\bar{q} = \frac{1}{2}\rho\|\boldsymbol{v}\|^2$ equation 5.6 can be reordered to develop the following equation for the equilibrium velocity:

$$\|\boldsymbol{v}\| = \sqrt{\frac{2m_T g\cos\theta}{\rho\left(C_{N_{wb}}A_r + C_{N_t}A_t\right)}} \tag{5.7}$$

By maximizing the denominator of equation 5.7 we find the smallest possible vehicle velocity that will maintain constant depth. This portion of the equation contains the information about the hydrodynamic surfaces and is maximized by increasing the lift coeffecient per AoA. This is done by adding a wing.

5.1.2 Wing Sizing

To maximize the vehicle lift, wings are used. To increase the lift per AoA we increase the ratio of wing span to vehicle radius $\frac{s}{r}$ found in the terms $\left(\frac{C_N}{C_{N_0}}\right)_{SB}$ and $\left(\frac{C_N}{C_{N_0}}\right)_{Newt}$ in equation 3.1. Adding wings allows the production of higher lift at a lower AoA. By decreasing the AoA needed to produce the lift force, a lower velocity can be reached before the stall angle is exceeded. Equation 5.7 is plotted in figure 5.2 for a variety of wing spans to show the effect of wing sizing on the relationship between equilibrium velocity and AoA. The increase of wing span shifts the velocity curve down. With the added wing area, a smaller angle of attack is required to maintain the same velocity.

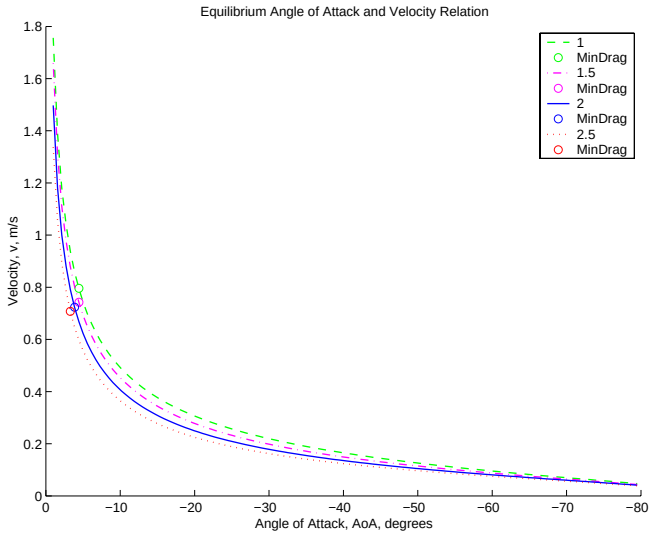

Figure 5.2: Velocity with minimum drag location

Unfortunately, adding additional hydrodynamic surfaces also adds drag to the system. When operating at cruise speeds outside of the low-speed regime, this added drag expends additional energy in cruise, limiting endurance. This total vehicle drag is shown in figure 5.3 where the minimum drag condition at low-speed is identified.

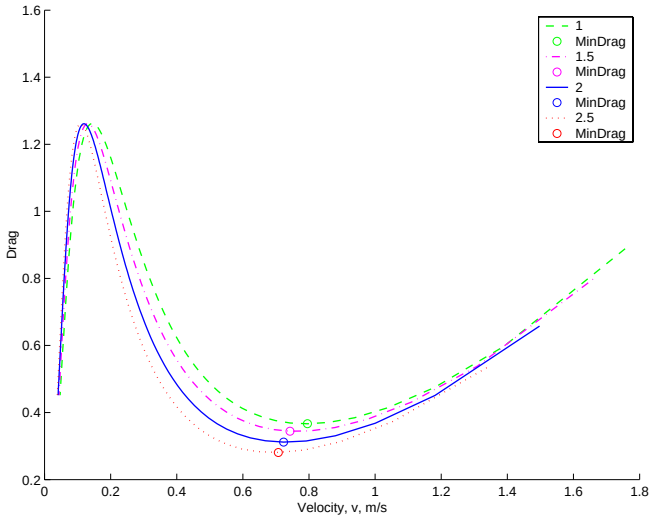

Figure 5.3: Minimum drag force

The most energy efficient travel condition for a winged vehicle is the point of maximum lift per unit of drag. This term, $\left(\frac{L}{D}\right)_{max}$, varies with velocity and wing span. How this condition changes with an increasing wing area is explored in figure 5.4.

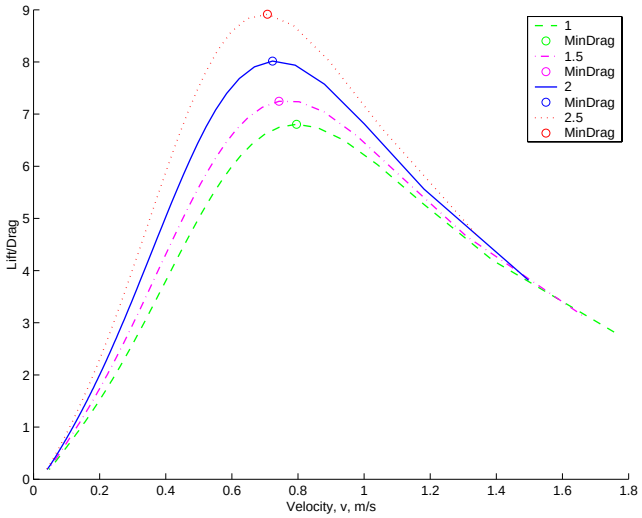

Figure 5.4: Lift to drag ratio with velocity

The question now arises, when should a wing be added to supplement the vehicle lift? To answer this question, we must know the desired lower velocity limit. Looking at the plot of the lift to drag ratio with AoA (fig. 5.5) we can see that $\left(\frac{L}{D}\right)_{max}$ occurs at low AoA ($\sim 4°$). For a loiter or low-speed inspection mission, the vehicle will maintain this

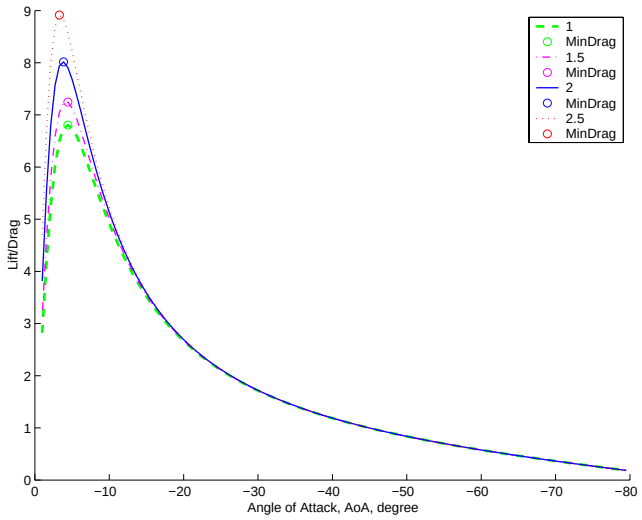

Figure 5.5: Lift to drag ratio with AoA

configuration for an extended period of time where vehicle efficiency will directly affect the vehicle operable time. In this case, the wing should be sized to yield the maximum lift to drag ratio at the desired velocity which happens to coincide with the minimum drag condition. Any speed above this velocity does not need wings to supplement the lift

and is therefore just adding drag to the system. However, low-speed vehicles that do fall into these velocity ranges can take advantage of the added lift at smaller AoA to drive slower and more efficiently.

5.1.3 Condition 2: $\Sigma M = P \times v$

Now we evaluate the second part of the equilibrium requirement (5.2).

$$\sum_{j=1}^{J} \boldsymbol{M_{ext_i}} = \boldsymbol{P} \times \boldsymbol{v} \tag{5.8}$$

The term $\boldsymbol{P} \times \boldsymbol{v}$ represents the inviscid flow Munk moment which arises due to the asymmetric location of the stagnation points. For motion in the longitudinal plane,

$$\begin{pmatrix} P_x \\ P_y \\ P_z \end{pmatrix} = \begin{pmatrix} (m_b + m_p + M_{f_x})u \\ 0 \\ (m_b + m_p + M_{f_z})w \end{pmatrix} \tag{5.9}$$

Substituting into 5.8 we find:

$$\begin{aligned} \boldsymbol{P} \times \boldsymbol{v} &= -\left((m_b + m_p + M_{f_x})uw - (m_b + m_p + M_{f_z})wu\right)\vec{\boldsymbol{j}} \\ &= \left(M_{f_z} - M_{f_x}\right)uw\vec{\boldsymbol{j}} \end{aligned} \tag{5.10}$$

Since $M_{f_z} > M_{f_x}$ for a slender body, this moment is destabilizing. We now define the sum of moments about the center of buoyancy in the following fashion:

$$\sum_{j=1}^{J} \boldsymbol{M_{ext_i}} = \boldsymbol{M_T} + \boldsymbol{M_p}$$

Here $\boldsymbol{M_T}$ is the sum of the hydrostatic and hydrodynamic moments on the vehicle and $\boldsymbol{M_p}$ represents the moment from the moving mass:

$$\boldsymbol{M_p} = \boldsymbol{r_p} \times m_p g \boldsymbol{R}^T \begin{pmatrix} 0 \\ 0 \\ 1 \end{pmatrix} [0\ 0\ 1]^T$$

For a single degree of freedom linear moving mass, r_{p_x} represents the travel length, r_{p_y} is assumed zero, and r_{p_z} is a constant that affects the pitch and roll stiffness of the vehicle and is further explained in section 5.1.4.

$$\begin{pmatrix} r_{p_x} \\ 0 \\ r_{p_z} \end{pmatrix} \times m_p g \begin{pmatrix} -\sin\theta \\ 0 \\ \cos\theta \end{pmatrix} = -m_p g \left(r_{p_x}\cos\theta + r_{p_z}\sin\theta\right)\vec{\boldsymbol{j}} \tag{5.11}$$

Equating this to the hydrostatic and hydrodynamic moments about the $\vec{j}$ axis allows a solution for the mass position (r_{p_x}) to be found.

$$(M_{f_z} - M_{f_x})\, uw = \boldsymbol{M}_T \cdot \boldsymbol{e}_2 - m_p g\,(r_{p_x} \cos\theta + r_{p_z} \sin\theta)$$

Reordering and solving for r_{p_x} yeilds:

$$r_{p_x} = \frac{\boldsymbol{M}_T \cdot \boldsymbol{e}_2 - (M_{f_z} - M_{f_x})\, uw}{m_p g \cos\theta} - r_{p_z} \tan\theta \tag{5.12}$$

This is the relation for the equilibrium position of the moving mass. Moving the mass to this location ensures that there is no resultant moment on the system.

5.1.4 The effect of r_{p_z}

Placing the moving mass below the vehicle lowers the overall center of gravity. With this low CG, the pitch dynamics can be roughly approximated through the motion of a pendulum.

$$\ddot{\theta} + b\dot{\theta} + \frac{mgr_{cg_z}}{I_{yy} + I_{f_y}} \sin\theta = \frac{\Sigma M_{pitch}}{I_{yy} + I_{f_y}} \tag{5.13}$$

Here the natural frequency of the undamped oscillation is given by:

$$\omega_y = \sqrt{\frac{mgr_{cg_z}}{I_{yy} + I_{f_y}}} \tag{5.14}$$

where the term under the radical is referred to as the pitch stiffness. This stiffness is directly proportional to the vertical distance from the center of rotation to the CG. A vehicle in this configuration (fig. 5.6), exhibits a reaction moment that fights propagation in θ. We now assume that the vehicle CG is coincendent with the CB. If the moving

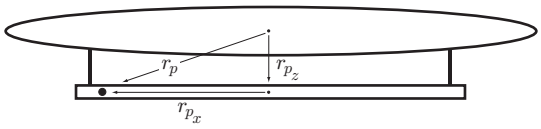

Figure 5.6: Low r_{p_z} effect

mass track goes though this point (fig. 5.7), the term $r_{p_z} = 0$. In this case, we start the moving mass at the marginally stable center point coincendent with both the CG and CB. Any mass movement forward from this point will attempt to bring the vehicle to a $-90°$ pitch to align the moving mass and the vehicle rotation center with the gravity vector. This characteristic is seen by looking at the moving mass moment equation.

$$\boldsymbol{M_p} = \boldsymbol{0} = \boldsymbol{r_p} \times m_p g \boldsymbol{R}^T [0\ 0\ 1]^T = m_p g\,(r_{p_x} \cos\theta + r_{p_z} \sin\theta)\,\vec{j}$$

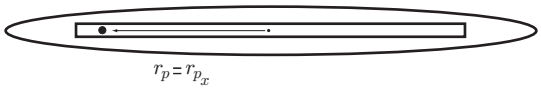

Figure 5.7: Low r_{p_z} effect

With a zero r_{p_z} the pitch moment is zero for all values of r_{p_x} at only $\theta = 90°, -90°$. With a nonzero r_{p_z} the pitch angle for a zero total moving mass pitch moment is given by:

$$\theta_{mp_0} = \tan^{-1}\left(-\frac{r_{p_x}}{r_{p_z}}\right)$$

Having a positive nonzero r_{p_z} affects the range of equilibrium pitch angles that is achievable though a change in r_{p_x}.

As r_{p_z} increases, the maximum controllable pitch angle decreases. This increase in vertical distance magnifies the passive pendulum stability through an increase in the pitch stiffness. This added stability can hinder rapid maneuverability and saturate hydrodynamic control surfaces.

Choosing a nominal r_{p_z} is a balance of satisfying maneuverability requirements and choosing a maximum controllable pitch angle for the vehicle. Because of the large decrease in lift upon reaching stall, this is an optimal choice for the largest controllable pitch angle. Now that we must consider the hydrodynamic moments we recall the evaluation of equation set 5.12. Requiring the total moment to be zero we find:

$$r_{p_{z_{optimal}}} = \frac{\boldsymbol{M}_{T_{stall}} \cdot \boldsymbol{e_2} - (M_{f_z} - M_{f_x})\, uw}{m_p g \sin\theta_{stall}} - \frac{r_{p_{x_{max}}}}{\tan\theta_{stall}}$$

A moving mass at this location $r_{p_{z_{optimal}}}$ maximizes the controllable pitch angle for the mass track length for a given velocity.

5.2 Sizing of the Horizontal Tail

We begin by recalling the primary destabilizing pitching moment of the wing-body (eqn. 3.3). This hydrodynamic moment varies quadratically with speed and is offset with a properly sized horizontal tail exhibiting the same quadratic velocity dependence. The moment generated from the horizontal tail depends on three factors. The lift curve slope, $C_{N_{\alpha_t}}$, modifiable through surface shape, roughness, thickness, etc. specifies the lift per unit area. The relation of the tail area (A_t) to the body area (A_r) denotes the proportional size of the tail lifting surface. Lastly, the longitudinal placement of the horizontal lifting

surface L_t as compared to the overall vehicle length describes the sign and magnitude of the moment. Grouping the latter two factors, the vehicle tail volume ratio is defined as:

$$\forall_t = \frac{L_t}{L}\frac{A_t}{A_r}$$

We furthermore define the pitching moment contribution of the horizontal tail as:

$$C_{m_t} = \forall_t C_{N_{\alpha_t}} (\alpha + \delta_e) \tag{5.15}$$

Assuming that the vehicle moment reference point is coincident with vehicle hydrodynamic center eliminates all velocity dependent moments except 3.3, which becomes:

$$C_m = \left[\left(\frac{\pi r}{4L}\right) \sin 2\alpha \cos\frac{\alpha}{2}\right] \left(\frac{C_m}{C_{m_0}}\right)_{SB} \tag{5.16}$$

To minimize drag we prefer a small horizontal tail. For this reason we choose the farthest stable location for the control surface, $L_t = -\frac{L}{2}$. By maximizing this distance, the ratio of areas can be minimized, resulting in a reduction of hydrodynamic drag at all angles. Equating 5.15 with 5.16 and solving for $\forall_t$ isolates the tail sizing variables from the nondimensionalized hydrodynamic coefficients.

$$\forall_t = \frac{C_{m_{wb}}}{C_{N_t}} \tag{5.17}$$

For a wingless body with a slenderness ratio of 15.5 the results of equation 5.17 are plotted as figure 5.8. We choose a value of tail volume ratio that will cover the peak of this plot to ensure at least marginal stability at all angles and all velocities. This value is chosen as a percentage of the small angle $\forall_t$ using the following equation:

$$\forall_t = 0.7\frac{\pi}{2}\frac{r}{L}\left[\left(\frac{s}{r}\right)^2 + \left(\frac{r}{s}\right)^2 - 1\right] \tag{5.18}$$

With correct sizing of the horizontal tail, the velocity dependent hydrodynamic moments are minimized with similar moments allowing the moving mass to remain effective under higher velocities.

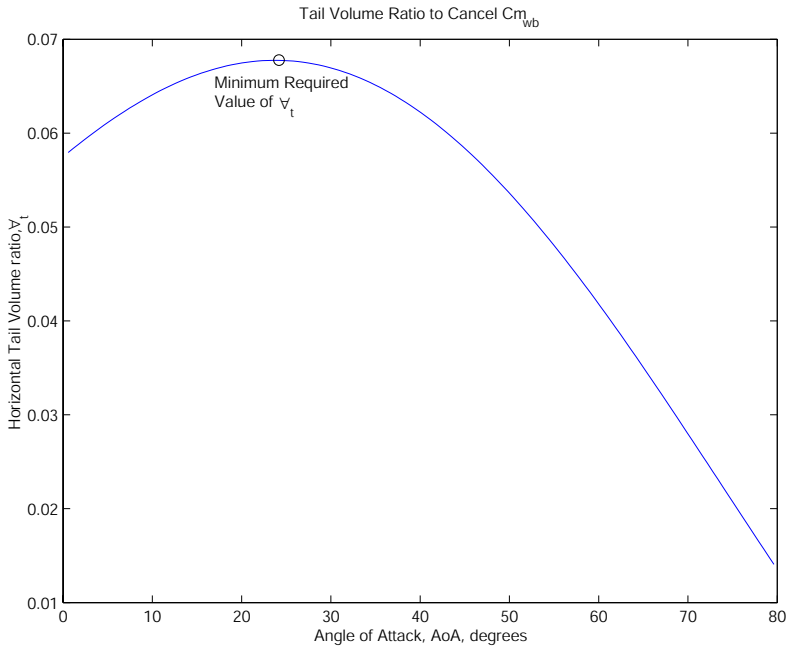

Figure 5.8: Relation between angle of attack and tail volume ratio

Chapter 6

Design of a Modular Moving Mass Actuator

6.1 Sizing and Shape

The moving mass actuator (MMA) was designed as an addition to the VTMAUV and was sized to be carried beneath the craft with the relative size, shape, and weight of the YSI payload sensor. This sized the approximate slenderness ratio and length of the moving mass controller. Iterations were taken from this point to size the actuator to operate effectively and safely. It was necessary to match the buoyancy percentage of the actuator to that of the vehicle to minimize any extra gravitational and buoyant forces. The buoyancy force of the slender cylindrical hull vehicle is defined as follows:

$$\frac{B}{W} = \frac{\pi r^2 L \rho g}{W}$$

which for the VTMAUV was approximately:

$$\frac{B}{W} \simeq \frac{\frac{1}{4}\pi \left(\frac{3.75}{12}\right)^2 \left(\frac{24}{12}\right) * 62.4}{5.52} = 1.73$$

The actuator itself is approximately 21 inches in length with an outer diameter of 1.75 inches resulting in a buoyancy force of:

$$B_{addon} \simeq \frac{1}{4}\pi \left(\frac{1.75}{12}\right)^2 \left(\frac{21}{12}\right) * 62.4 = 1.82\ lbs$$

Using this buoyancy force we can calculate how much the modular addition must weigh to maintain the same buoyancy ratio as the vehicle.

$$W_{addon} \simeq \frac{B_{addon}}{\left(\frac{B}{W}\right)} = \frac{1.82}{1.73} = 1.05\ lbs$$

This is the necessary weight for the craft to maintain the same buoyancy factor as the vehicle. The VTMAUV was designed to carry a heavy payload, and because of this, the weight requirement is not a critical issue, provided the sum of the moving mass and vehicle system remains positively buoyant. If the actuator is developed with a higher net buoyancy than the craft, the actuator in conjunction with the craft would become more buoyant, adversely affecting the lower velocity limit. Adding additional positive buoyancy low on the craft will also lower the center of buoyancy creating a loss of roll stability.

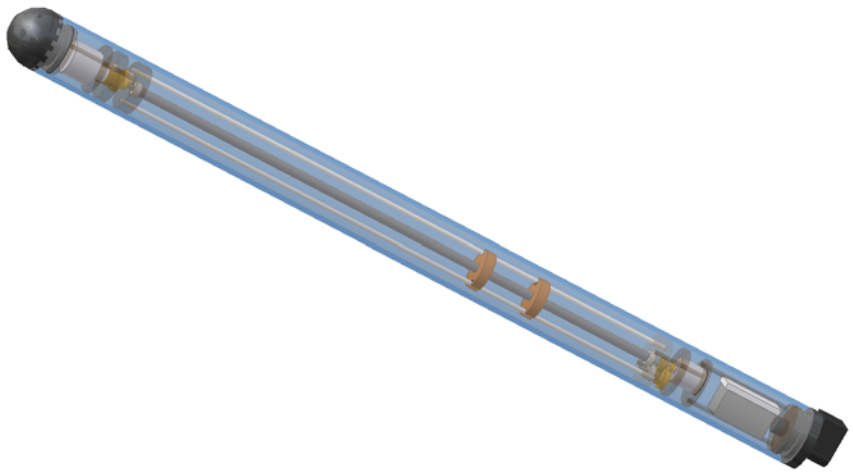

Figure 6.1: Assembled moving mass

6.2 Materials

The MMA was designed for the same depth and environment as the VTMAUV and because of this, uses many of the same types of materials. The outside casing is the only material that interacts with the fluid medium. Compressive effects from depth, as well as corrosive effects must be considered in material selection. A clear acrylic tube of 1.75 inches outer diameter and 1.5 inches inner diameter was used for this purpose. The hull transparency allows the user to visually inspect the apparatus allowing problems to be quickly identified on a test stand if they occur. A 10-pin wet-mateable connector is used

to communicate with the craft through RS232 serial protocol. This connector is sealed from leaking through a pressure fitting that screws into the rear end cap. The forward and aft end caps are both opaque delrin and, like the acrylic, are chemically inert in water. These caps are sealed with O-rings to prevent any leaking at depth.

The primary drive is an ACME stainless steel lead screw. The ACME lead nuts used to position and hold the mass are brass, primarily used for its density and self lubricating properties. Anodized aluminum rods run the mass area to keep the brass nuts from turning with the lead screw. The nylon spacers provide a solid mounting location for the brass gear train in the aft and the titanium gear train in the front. The titanium gears were cannibalized from a HiTec high torque servo motor from which the servo motor and circuit board were used.

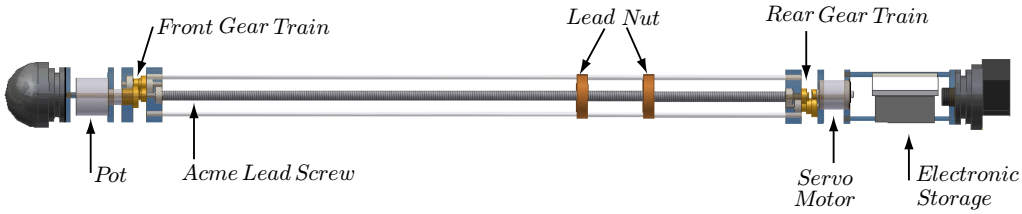

Figure 6.2: Part breakdown of MMA

6.3 Mechanism

Creating a linear motion using a rotating motor is accomplished using a lead screw and two geared transmissions. A 3 turns per inch, $\frac{1}{4}$ inch diameter ACME lead screw was used to move the mass. Two brass machinable round nuts were cut to $\frac{1}{2}$ inch thickness and notches were placed to follow anodized aluminum guardrails that prevented the mass assembly from rotating with the lead screw. These two round nuts guide the mass along the track by sandwiching the mass and bolting to each other. To minimize the amount of mass needed, the mass must be moved as far as possible from the center of rotation to induce a larger pitching moment, therefore the travellable length of the mass must be maximized.

6.3.1 Front Transmission

The primary limitation of the moving mass travel length is the 10-turn potentiometer. If hooked directly to the lead screw the hard limits on the potentiometer would only allow

about $3\frac{1}{3}$ inches of travel. The solution to allowing the mass to move farther is to design a geared transmission between the lead screw and the potentiometer. This gearing ratio is determined by the desired travel length, the gears available, and the physical sizing restrictions inherent from operating in a sealed vessel. Figure 6.3 shows the designed transmission as well as the gears used. All of the gears are made of brass. They were

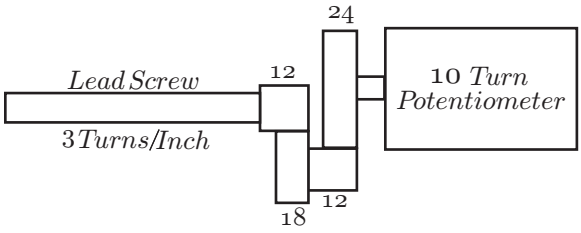

Figure 6.3: Front gearing to maximize travel length (numbers shown are number of gear teeth)

purchased in 12, 18, and 24 tooth sizes with a 48 pitch. One 18 and one 12 tooth gear were fastened together to ensure that they would rotate at the same rate. This double gear does not change the gearing ratio but instead links the remaining gears while keeping the overall total gear-face area minimized. The total travel length is calculated using the following equation:

$$10\ turns\left(\frac{24}{12}\right)\left(\frac{18}{12}\right)\left(\frac{1}{3\frac{turns}{inch}}\right) = 10\ inches$$

The track has an overall length of $14\frac{1}{4}$ inches leaving $2\frac{1}{8}$ inches of free space on either side of the extremes. Using all of this space yields a total overall mass length of $3\frac{3}{4}$ inches. The masses used were constructed in the shape shown in figure 6.4 so that they could be inserted sideways between the guiding rods and turned 90° to lock into the right location. These masses are suspended on two small rods that connect the two brass nuts

Figure 6.4: Shape of mass segments

and are secured with a small pin at each end. This method was chosen to prevent extra bending on the nuts themselves which increases the possibility of binding in the system.

These small rods keep the mass sections off of the lead screw and distribute the load between the two lead nuts. Now that the length and mass movement properties have been addressed it is necessary to magnify the torque of the motor so that the system can be driven.

6.3.2 Rear Transmission

The rear transmission is primarily designed to amplify motor torque so that the system can overcome inherent frictional losses. This set of gears use the titanium gears from the cannibalized HiTec high torque servo motor. This fact limited the assembly options due to the limited size and number of each gear. Using the provided materials, the smallest outer diameter and highest torque magnification was created allowing the highest possible magnification of torque. This front transmission is shown in Figure 6.5. The number of

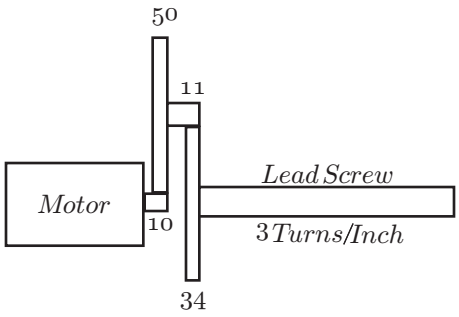

Figure 6.5: Rear gearing to increase motor torque (numbers shown are number of gear teeth)

teeth were counted on each gear and matched with the gears of a compatible pitch. The torque amplification was calculated by looking at the number of motor turns necessary for the shaft to turn once:

$$\left(\frac{34}{11}\right)\left(\frac{50}{10}\right) = \frac{170}{11} \simeq 15.45$$

The torque of the motor is amplified approximately 15.5 times. The HiTec high torque servo motor originally had a torque value of 250 oz-in at 4.8 volts after being run though a gearing ratio of 49.93. By reconfiguring the gears we now maintain approximately 30 percent of that torque resulting in a torque of 77.36 oz-in with a 4.8 volt power input or 103.04 oz-in with a 6 volt power input. The Acme lead screw was specifically chosen because of the low frictional torque between the screw and nut. This friction is the primary opposing torque and when combined with the frictional losses in the gears themselves presents the overall torque that the motor must overcome.

6.4 Electronics

The primary electronic hardware was cannibalized from the Hitec high torque servo motor. Using the embedded driver chip, the potentiometer was replaced with a multiturn potentiometer, minimizing the gearing ratio needed to achieve a reasonable travel distance. This servo motor takes a pulse width modulated signal and the driver chip relates the width of the pulse to a certain value on the potentiometer. The motor then operates in the appropriate direction until the commanded potentiometer value is reached. To interface between the computer of the mother vessel and the modified servo motor, an Object Oriented PIC (OOPic) microprocessor was utilized. This OOPic can be seen in Figure 6.6. Accepting a RS232 serial connection from the mother vessel, the actuator

Figure 6.6: The Object Oriented Pic C variant (OOPic-C))

runs though the Basic code shown in Appendix 8.1. The smallest form of the OOPic is used (C variant) because it was the only chip that could provide the level of programming preferred while occupying a relatively small volume. This chip accepts a direct RS232 9 volt signal internally converting to the lower 5 volt TTL language for the chip level communication. The RS232 form of communication is preferred over direct TTL communication for the stability of the signal over long distances. The OOPIC additionally accepts digital and analog sensory inputs that can be utilized for a variety of sensory platforms. One of these analog connections was connected in line with the variable voltage line on the potentiometer so that some position identification can be read directly back to the mothership.

The code in appendix 8.1 accepts a 0-63 integer command corresponding with 64 stations along the travel length of the mass. If an integer value 0-63 is sent though the RS232 line the modified servo will move to the corresponding location. A value outside of this range, such as 64, will instead request the current location of the mass from the system. This is a method of checking to ensure that the mass arrived at the correct location. A green light emitting diode (LED) is connected to the 31st digital I/O line and is turned on when the motor is commanded to move. This provides a method of checking that the code is running if troubleshooting is needed. The electronic circuit board that ties these components together is shown in Figure 6.7. Using a 10-pin wet-mateable male connector, the actuator is linked to the mothership. Only 4 of the 10 available lines are

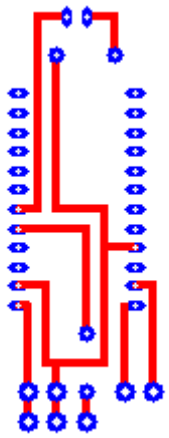

Figure 6.7: Electric circuit diagram for electronics

used following the pinout found in table 6.1.

Table 6.1: Pinout for actuator connection interface

Pin	Connection
5	5 volt power
6	R_x, RS232 Receive
7	T_x, RS232 Transmit
8	Ground

Here the 5 volt source powers both the OOPic and the motor from the onboard power of the mothership. To minimize the actuator's impact on the battery life of its host vehicle, the actuator only draws significant power while moving. When the mass reaches its destination the motor is powered down while the OOPic waits for the next command. Because the servo motor and the OOPic use a common power source, two additional electrical issues must be addressed. A DC motor uses principles of electromagnetics to create a magnetic field that spins a core of metal windings thus turning a shaft. When the power is cut on the motor, these windings maintain some rotational inertia, and continue to spin until brought to a stop through frictional losses. While the motor spins its generates a voltage that, if not blocked or dissipated, travels back to the power source. This is referred to as back-emf and can be detrimental to a system that can not accommodate the reversal of voltage. Most rechargeable battery types can handle this phenomenon with little problem by absorbing the excess energy from the motor. If

back-emf becomes a problem it is most often eliminated though use of a diode and a system of resistors.

The second problem that needs attention is the voltage spike associated with a command to the motor. Certain battery types such as the new Lithium-Ion batteries have current limiting embedded chips that cut power if a voltage spike exceeds some limit. If this occurs, power is severed from the craft often rebooting the system, losing information, control, and time. This can be avoided by using batteries that can absorb these voltage spikes. Examples of these types of batteries include Nickel-Metal-Hydride (NiMHs) and Nickel-Cadmium (NiCADs) batteries. These don't have as high of an overall power density as the Lithium-Ion but are more robust to electric deviations.

Chapter 7

Experimental Testing

Testing of the moving mass actuator was performed with the VTMAUV in Panama City, Florida on June 24th 2005. The MMA was secured below the AUV and ballasted so that the assembly sits level in the water with the moving mass centered at position 30. To verify that the VTMAUV could operate over the entire range of moving mass positions, the vehicle was commanded to swim at it's nominal speed of 1 m/s and to maintain a depth of 1.5 meters in a series of experiments for which the moving mass was fixed at various locations. After verifying that the VTMAUV remained controllable through all MMA positions a dynamic test was performed. In all experiments, a separate PID feedback loop actuated the fins to maintain the specified depth.

7.1 Fixed MMA Positions

A series of 14 runs were performed with the moving mass fixed at 7 known positions. In each test the depth, fin commands, and attitude histories were recorded. These time dependent states were plotted in the manner shown in figure 7.1 where the cruise steady-state values were identified. Once the VTMAUV achieved a steady-state depth, the state histories were filtered and cut to incorporate only the sections of cruise. These sections are plotted and appear as in figure 7.2. Upon reaching this range of values, the resulting equilibrium pitch, roll, and fin deflections were averaged. These approximate equilibrium averages are shown for each mass location in table 7.1. The three fin configuration of the VTMAUV is shown in figure 7.3. The discrepancy between Fin_a and Fin_b is due to the induced roll moment from the propeller. As the moving mass travels from its rearmost location forward, the fins compensate for the added CG offset. As seen in figure 7.4, the PID-controlled fins compensate for the changing gravitational moment.

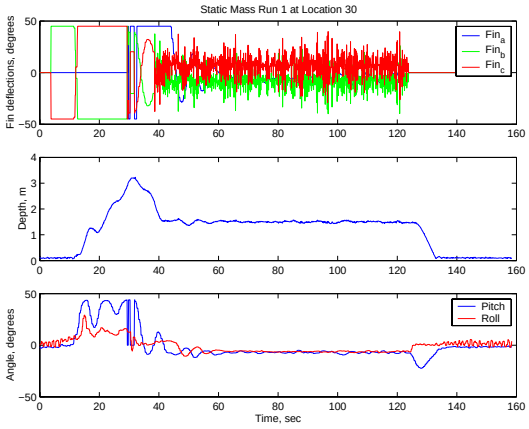

Figure 7.1: Full set of unfiltered dynamic data taken with MMA at position 30. (In the top plot, the solid line represents Fin_a, the dashed line represents Fin_b, and the dotted line represents Fin_c. In the bottom plot, the solid line represents pitch angle and the dotted line represents roll angle.)

Table 7.1: Equilibrium conditions at mass locations

MMA Location	Depth	Pitch	Roll	Fin_a	Fin_b	Fin_c
2	1.50	-11.30	-4.47	10.08	11.72	-4.61
10	1.50	-9.81	-4.54	5.84	8.20	-1.09
20	1.50	-8.26	-5.05	4.33	4.02	3.09
30	1.50	-7.85	-6.16	-0.81	-2.66	9.76
40	1.50	-6.48	-5.44	-1.54	-5.76	12.86
50	1.50	-5.70	-6.72	-3.55	-8.28	15.38
60	1.54	-5.59	-8.58	-6.61	-11.15	18.26

The vehicle is trimmed so that, for a moving mass location of 30, the CG is longitudinally aligned with the CB. Smaller (more rearward) mass locations generate a nose-up gravitational moment which must be countered by the the tail fins to maintain a nose-down attitude. Larger (more forward) mass locations require less moment of the tail fins up to the point where the nose-down attitude exceeds the trim condition, at which point the fins must generate a nose-up moment. At this critical mass location, the fins become unnecessary as the entire equilibrium pitch control moment is generated by the MMA. This observation is particularly important for control at lower speeds, where the fins might be incapable of generating the necessary equilibrium pitch control moment.

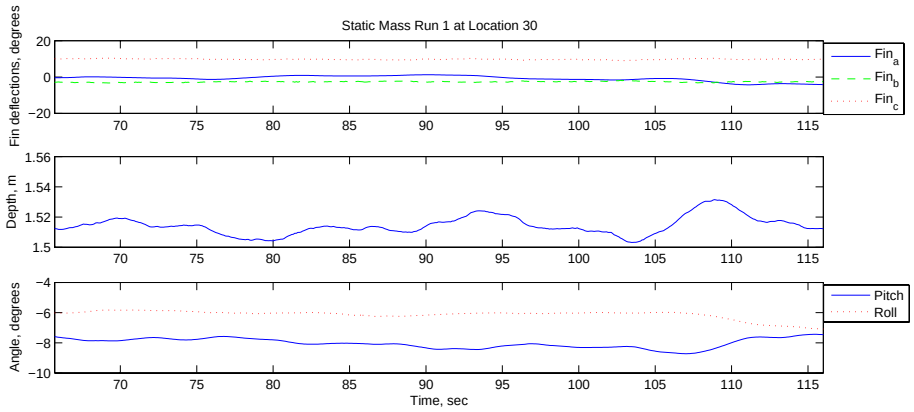

Figure 7.2: Filtered and trimmed dynamic data taken with MMA at position 30. (In the top plot, the solid line represents $\mathrm{Fin_a}$, the dashed line represents $\mathrm{Fin_b}$, and the dotted line represents $\mathrm{Fin_c}$. In the bottom plot, the solid line represents pitch angle and the dotted line represents roll angle.)

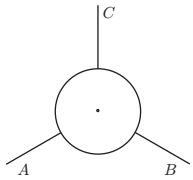

Figure 7.3: VTMAUV fin orientation,viewed from the front.

7.2 Dynamic Run

The vehicle was next programmed to maintain depth with the moving mass at its rearward-most position, allowing sufficient time to achieve steady state, after which the mass was slewed to its forward-most location. Again the vehicle was programmed to travel at its design speed of 1 m/s. The control, depth, and attitude histories are shown in Fig. 7.5, where the vertical dashed line indicates the beginning of the moving mass transition. As the mass moves forward, the vehicle pitches nose-down and dives slightly. Eventually, once the mass has reached its forward-most position, the PID depth controller brings the vehicle back to its specified depth. Initially, the tail fins are deflected leading edge up to generate a nose-down moment. The local lift generated by the fins is therefore upward and must be opposed by additional down force on the vehicle hull. Thus, the trim pitch angle is more negative at the beginning of the experiment. As the tail fins adjust to the forward-moving CG, they generate less upward force and, eventually, begin generating downward force. As a result, the equilibrium pitch angle becomes

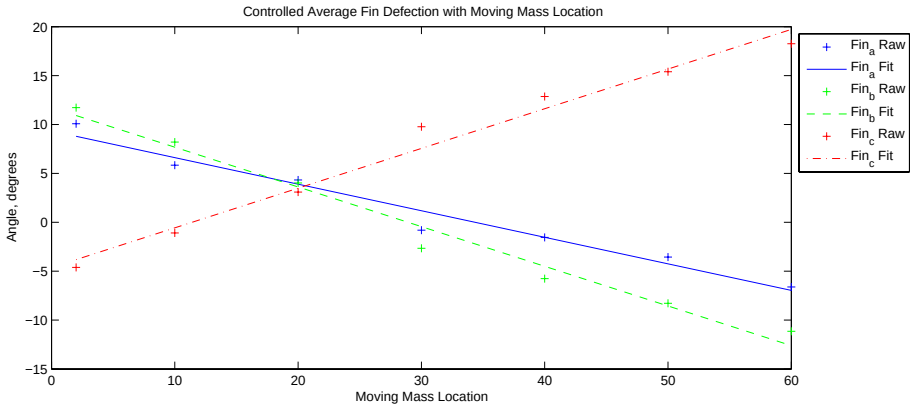

Figure 7.4: Equilibrium fin locations with commanded MMA locations. (The solid line represents a linear fit to the Fin_a. The dashed line represents a linear fit to the Fin_b. The dash-dotted line represents a linear fit to the Fin_c.)

less negative because less down force must be generated by the hull.

From one point of view, the dynamic data shown in Fig. 7.5 illustrate the VTMAUV depth controller's ability to reject steady pitch disturbances. Viewed another way, the data illustrate the MMA's effectiveness at generating a pitch control moment. Moreover, because this control moment is independent of vehicle speed, the MMA should also be effective for depth control at low speeds.

7.3 Diving

An added advantage to dynamically controlling the vehicle center of gravity becomes apparent when trying to autonomously submerge a positively buoyant AUV. The VTMAUV currently dives by reversing the propeller and driving backwards until enough of the propeller is submerged to pull the vehicle underwater. The vehicle the reverses thrust to drive forward. Using the moving mass in a rear position during this section of the vehicle flight profile adds a gravitational moment that aids in the submersion of the propeller. In the case of the VTMAUV, the MMA in the rearmost position fully submerged the propeller, allowing immediate submergence. Controlling this initial propeller submergence leads to a quicker $\dot{z}$ and a steeper diving trajectory unavailable through use of fins alone. Because of the steep diving trajectory and the positively buoyant nature of the vehicle, the depth will overshoot the desired depth. The magnitude of this overshoot is a function of the net buoyancy of the AUV, the response speed of the MMA, the agility of the primary thruster, and actuation speeds of the control surfaces.

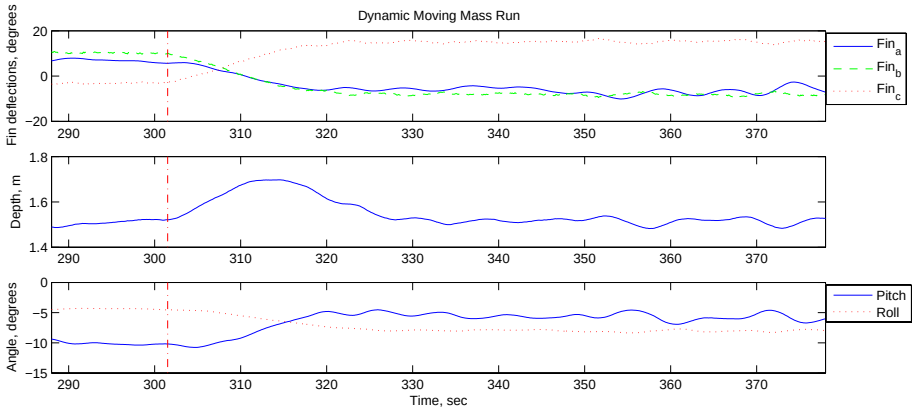

Figure 7.5: Vehicle response to slewing the moving mass from its full rearward to its full forward position. The transition begins at $t = 301.5$ seconds. (In the top plot, the solid line represents Fin_a, the dashed line represents Fin_b, and the dotted line represents Fin_c. In the bottom plot, the solid line represents pitch angle and the dotted line represents roll angle.)

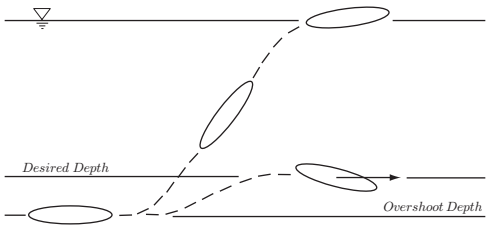

Figure 7.6: Reverse diving proceedure

Alternatively, the AUV can use the MMA to dive in a nose forward manner more conducive to shallow water diving. This is accomplished by using the internal momentum of the moving mass actuator to quickly go from a rear position where the propeller is submerged and effective, to a full forward position causing the vehicle to arc forward. With enough vehicle momentum, the AUV will carry itself underwater nose first and dive

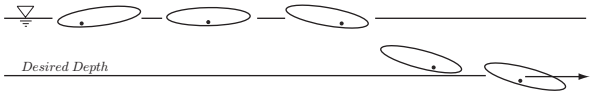

Figure 7.7: Forward or breaching diving proceedure

sufficiently far to resubmerge the propeller.

7.4 Parameter Identification

The averaged steady-state data collected in the previous experiments can be used to produce a better estimate of the hydrodynamic and gravitational parameters. Recognizing that all of the angles in table 7.1 are small, a linearized estimate of the hydrodynamic parameters is reasonable. Recalling the equilibrium conditions 5.1 and 5.2, the following linearized equations can be formulated:

$$\begin{aligned} C_B - C_W &= C_{N_{\theta_{wb}}}\theta + 2\frac{A_t}{A_r}C_{N_{\delta_e}}(\theta + \delta_e) + C_T\theta \\ -\frac{m_p g}{\bar{q}A_r}\left(\frac{r_{p_{x_i}}}{L} + \frac{r_{p_z}}{L}\theta_i\right) &= C_{M_\theta}\theta + 2\frac{A_t}{A_r}C_{M_{\delta_e}}(\theta_i + \delta_{e_i}) \end{aligned}$$

Here the variables $C_{N_{\theta_{wb}}}, C_{N_t}, C_T, C_{M_\theta}, C_{M_{\delta_e}}$ and $C_{M_{\delta_{cg}}}$ are solved through simultaneous equations using the previously collected empirical data. Placing this information into the matrix form, $\boldsymbol{Ax} = \boldsymbol{B}$, yields:

$$\boldsymbol{A} = \begin{bmatrix} \theta_1 & 2\frac{A_t}{A_r}(\theta_1 + \delta_{e_1}) & \theta_1 & 0 & 0 & 0 \\ \theta_2 & 2\frac{A_t}{A_r}(\theta_2 + \delta_{e_2}) & \theta_2 & 0 & 0 & 0 \\ \vdots & \vdots & \vdots & \vdots & \vdots & \vdots \\ 0 & 0 & 0 & \theta_1 & 2\frac{A_t}{A_r}(\theta_1 + \delta_{e_1}) & \delta_{cg_1} \\ 0 & 0 & 0 & \theta_2 & 2\frac{A_t}{A_r}(\theta_2 + \delta_{e_2}) & \delta_{cg_2} \\ \vdots & \vdots & \vdots & \vdots & \vdots & \vdots \end{bmatrix}$$

$$\boldsymbol{B} = \begin{pmatrix} (C_B - C_W) \\ (C_B - C_W) \\ \vdots \\ -\frac{m_p g}{\bar{q}A_r}\left(\frac{r_{p_{x_1}}}{L} + \frac{r_{p_x}}{L}\theta_1\right) \\ -\frac{m_p g}{\bar{q}A_r}\left(\frac{r_{p_{x_2}}}{L} + \frac{r_{p_z}}{L}\theta_2\right) \\ \vdots \end{pmatrix}$$

where

$$\boldsymbol{x} = \begin{pmatrix} C_{N_{\theta_{wb}}} \\ C_{N_{\delta_e}} \\ C_T \\ C_{M_{\theta_{wb}}} \\ C_{M_{\delta_e}} \end{pmatrix}$$

The matrix $\boldsymbol{A}$ is not necessarily square and is inverted using the pseudoinverse. If the

Table 7.2: Least squares solution using the data from Table 7.1 and the VTMAUV physical approximations. $\frac{A_t}{A_r} = 0.3$, $\frac{r_{pz}}{L} = 0.01$

Variable	Value
$C_{N_{\theta_{wb}}}$	-0.0014
$C_{N_{\delta_e}}$	-0.0018
C_T	-0.0014
$C_{M_{\theta_{wb}}}$	-4.1438
$C_{M_{\delta_e}}$	7.0789

inverse of $\left(\boldsymbol{A}^T\boldsymbol{A}\right)$ exists, the Moore-Penrose inverse [28] can be defined as:

$$\boldsymbol{A}^\dagger = \left(\boldsymbol{A}^T\boldsymbol{A}\right)^{-1}\boldsymbol{A}^T$$

Use of this term in the equation: $\boldsymbol{x} = \boldsymbol{A}^\dagger\boldsymbol{B}$ locates the least squares solution to the problem $\boldsymbol{A}\boldsymbol{x} = \boldsymbol{B}$.

Using a rough approximation for the physical dimensions of the VTMAUV yields the coefficients found in table 7.2. The signs of $C_{N_{\theta_{wb}}}$, $C_{N_{\delta_e}}$, C_T show a positive force when coupled with a negative θ and δ_e which is expected for a positively buoyant submersible. The value $C_{M_{\theta_{wb}}}$ is negative and large suggesting a very statically stable system for the chosen tail area over the range of moving mass positions. These equations illustrate the use of a MMA to determine an estimation of the hydrodynamic parameters which are often difficult to empirically identify. The Matlab code created to solve this problem is presented in section 8.3.

Chapter 8

Conclusions & Recommendations

Streamlined AUVs are typically trimmed to be somewhat buoyant or heavy in water. To maintain depth, they must generate a constant hydrodynamic force which requires that they swim at a constant pitch angle. Although tail fins are the typical mechanism for generating this control moment, they become ineffective at low speeds. To enable an existing AUV to travel at lower speeds, one may easily incorporate a modular moving mass actuator. In some cases, it may also be advantageous to include a fixed wing.

The dynamic effects of the moving mass were evaluated to develop the equations of motion. The equilibrium conditions necessary to maintain a constant depth and velocity were defined, and the effectiveness and low-speed efficiency of a fixed wing was analyzed. An expression was derived to determine whether a wing is needed to travel with peak efficiency for a given speed. The effect of the vertical offset of the moving mass was analyzed to establish the relation between the control angle and the moving mass linear position. Sizing guidelines were constructed for sizing of the horizontal tail and placement of the MMA below the AUV centerline.

A description of the design of a one degree of freedom moving mass actuator module and preliminary experiments using the Virginia Tech Miniature AUV was provided. Data was presented for a series of fixed MMA position experiments as well as a dynamic position test. The results illustrate the effectiveness of a moving mass actuator at generating low-speed control moments. With the collected data, parameter identification was performed to get an estimate on the hydrodynamic parameters.

Planned experiments should further demonstrate the actuator's ability to control an AUV at an otherwise uncontrollably low speed.

References

[1] Christopher von Alt, "Autonomous underwater vehicles," *Autonomous Underwater Lagrangian Platforms and Sensors Workshop*, March 2003. 3

[2] Terry Ewart, "Observations from straight line isobaric runs of SPURV," 3

[3] Terry Ewart and W. Bender, "An observation of the horizontal and vertical diffusion of a passive tracer in the deep ocean," *Journal of Geophysical Research*, vol. 86, pp. 10,974–10,982, November 1981. 3

[4] James M. Walton and Richard W. Uhrich, "114 unteathered UUV dives: Lessons learned," *MTS/IEEE Oceans95*, 1995], month = October,. 3

[5] D. L. Endicott and G. R. Khul, "Epulard:deep bottom surveys now with acoustic remote controlled vehicle, first operational experience," tech. rep., Proceedings of Oceans 81, Boston, MA, September 1981. 3

[6] J. Bellingham, C. Goudey, and C. Chryssostomidis, "A small long range autonomous vehicle for deep ocean exploration," *Proceedings of the 2nd International Offshore and Polar Engineering Conference*, 1992. 4

[7] T. Curtin, J. Bellingham, and D. Webb, "Autonomous oceanographic sampling networks," *Oceanographics*, 1993. 4

[8] B. Butcher and M. Black, "The Theseus autonomous underwater vehicle - two successful missions," in *Proceedings from the 10th International Symposium on Unmanned Un-tethered Submersible Technology*, pp. 12–22, Autonomous Undersea Systems Institute. 4

[9] C. von Alt, B. Allen, and T. Austin, "Remote environmental measuring units," in *Autonomous Underwater Vehicle Conference*, (Cambridge, MA), 1994. 4

[10] G. Griffiths and K. Birch, "Oceanographic surveys with a 50 hour endurance autonomous underwater vehicle," in *Proceeding of the Offshore Technology Conference*, (Houston, TX), May 2000. 4

[11] H. Stommel, "The Slocum mission," *Oceanography*, vol. 2, pp. 22–25, April 1989. 4

[12] Douglas C. Webb, Paul J. Simonetti, and Clayton P. Jones, "SLOCUM: An underwater glider propelled by environmental energy," *IEEE Journal of Oceanic Engineering*, vol. 26, pp. 447–452, October 2001. 5

[13] Jeff Sherman, Russ E. Davis, W.B. Owens, and J. Valdes, "The autonomous underwater glider "Spray"," *IEEE Journal of Oceanic Engineering*, vol. 26, pp. 437–446, October 2001. 5

[14] Charles C. Eriksen, T. James Osse, Russel D. Light, and Timothy Wen, "Seaglider: A long-range autonomous underwater vehicle for oceanographic research," *IEEE Journal of Oceanic Engineering*, vol. 26, pp. 424–436, October 2001. 5

[15] Leonard, Naomi E. and Graver, Joshua G., "Model-based feedback control of autonomous underwater gliders," *IEEE Journal of Oceanic Engineering*, vol. 26, pp. 633–645, October 2001. 5

[16] Wick, C. E. and Stilwell, D. J., "USNA-1: A Miniature, Low-Cost, Autonomous Underwater Vehicle," *Sea Technology*, vol. 43, no. 6, pp. 17–25, 2002. 5

[17] Gadre, A. S., Mach, J. J., Stilwell, D. J., and Wick, C. E., "Design of a prototype miniature autonomous underwater vehicle," in *Proceedings of the IEEE/RSJ Intelligent Robotics and Systems*, (Las Vegas, NV), pp. 842–846, 2003. 5

[18] J. H. McMasters, "An analytical survey of low-speed flying devices - natural and man-made," *Technical Soaring*, vol. 3, no. 4, pp. 17–42, 1975. 5

[19] G. S. Triantafyllou, M. S. Triantafyllou, and M. A. Grosenbauch, "Optimal thrust development in oscillating foils with application to fish propulsion," *J. Fluids Struct.*, vol. 7, pp. 205–224, 1993. 8

[20] D. Barrett, M. Grosenbaugh, and M. Triantafyllou, "The optimal control of a flexible hull robotic undersea vehicle propelled by an oscillating foil," in *IEEE AUV Symp.*, 1996], organization = IEEE,. 8

[21] George V. Lauder and Eliot G. Drucker, "Morphology and experimental hydrodynamics of fish fin control surfaces," *IEEE Journal of Oceanic Engineering*, vol. 29, pp. 556–571, July 2004. 8

[22] C. A. Woolsey and N. E. Leonard, "Stabilizing underwater vehicle motion using internal rotors," *Automatica*, vol. 38, pp. 2053–2062, June 2002. 9

[23] Hanspeter Schaub and John L. Junkins, *Analytical Mechanics of Space Systems*. Virginia Polytechnic Institute and State University: American Institute of Aeronautics and Astronautics, Inc., 2003. 9

[24] Leland H. Jorgensen, "A method for estimating static aerodynamic characteristics for slender bodies of circular and noncircular cross section alone and with lifting surfaces at angles of attack from 0° to 90°," Tech. Rep. NASA TN D-7228, Ames Research Center, Moffett Field, Calif. 94035, April 1973. 15

[25] Hoerner, Sighard F., *Fluid-Dynamic Lift*. Brick Town, NJ: Hoerner Fluid Dynamics, 1975. 17, 25

[26] Charles Smith Jr., "The effects of fuel sloshing on the lateral stability of a free-flying airplane model," tech. rep., NACA: Langley Memorial Aeronautical Laboratory, Langley Field, VA, June 1948. 19

[27] Thor I. Fossen, *Guidance and Control of Ocean Vehicles*. West Sussex, England: John Wiley and Sons, 1994. 24

[28] Campbell, S.L. and Meyer, C.D. Jr., *Generalized Inverses of Linear Transformations*. New York: Dover, 1991. 53

Appendix

8.1 OOPic Code

```
Dim Pot As New oA2D
Dim Servo As New oServo
Dim Target as New oByte
Dim RS232 As New oSerial
Dim LED As New oDio1
Dim storage1 as New oByte          'intermediate value holder
Dim storage2 as New oByte          'Final value holder
Dim subber as New oByte            'sensor subtract argument
Dim joiner as New oMath            'Linking object
Dim divide as New oByte            'Noise masking argument
Dim jitter as New oMath            'Used to mask off lower bits

Sub Main()
OOPic.Node = 1
LED.IOLine = 30
LED.Direction = cvOutput
Call SetupMotor
Call initcomm
Do
    If RS232.Received = cvTrue THEN
    Target.value = RS232.Value
        If (Target.Value <= 63) and (Target.Value >= 0) then
            Servo.Operate = cvTrue        ' Turn the servo on.
            LED.Value = 1
            Servo.Value = Target.Value
            OOPic.delay = 200
            Servo.Operate = cvFalse       ' Turn the servo off.
            LED.Value = 0
        else
            Call potcalc
            RS232.String = Str$(Storage2)
            RS232.Value = 13
```

```
            RS232.Value = 10
            RS232.String = Str$(Pot.value)
            RS232.Value = 13
            RS232.Value = 10
        End If
    End If
Loop
End Sub

Sub SetupMotor()
    Servo.IOLine = 31                   ' Specify the I/O Line.
    Servo.Center = 28                   ' Specify the center.
    Pot.IOLine = 1
    Pot.Operate = cvTrue
End Sub

Sub initcomm()
    RS232.Baud = cv9600
    RS232.Operate = cvTrue
End Sub

Sub potcalc()
    subber = 18                         'Subtract 18

    joiner.Input1.Link(Pot)             'Get sensor data
    joiner.Input2.Link(subber)          'scale value down
    joiner.Output.Link(storage1)        'Put it to temp. storage1
    joiner.Mode = cvSubtract            'Subtract 2 from 1
    joiner.Operate = cvTrue

    divide = 1 'divisor

    jitter.Input1.Link(storage1)        'Get result of last math
    jitter.Input2.Link(divide)          'get divisor
    jitter.Output.Link(Storage2)        'Put it to temp. storage2
    jitter.Mode = cvRShift              'divide by two
    jitter.Operate = cvTrue
End Sub
```

8.2 Static Matlab Code

```
%Model
% close all
% clear
% clc

global tstep td e1 rho g rpy rpz mb mp rp rcg L Ib Ab Ap Ar CNCN0SB
 CNCN0Newt CDn CA0 Vol CLa_fin CD0_fin AR_fin e_fin St xac xt xv
 mbuoy k1 k2 kp findeflh xbold xt n finlimit
place rpdes

I = eye(3); e1 = I(:,1); e2 = I(:,2); e3 = I(:,3);

%%%%%%%%%%%%%%%%%%%%%%%%%%%%%%%%%%%%%%%%%%%%%%%%%%%%%%%%%%%%%%%%%%%%%%%
r = 3.75/2*.0254;   %Radius of cylindrical hull
s_r = 2.5;            %Ratio of Wingspan to radius 1 for no wings
L_r = 15.5;         %Ratio of Vehicle Length to radius

%CG offset
xcg_L = 0.01; zcg_L = 0.02; xac_L = 0.0; zac_L = 0;

%Fins
Lt_L = 0.5+xac_L;       % Ratio of distance from vehicle AC to
                        % horizontal tail AC to Total length
St_S = 0.3;             % Ratio of Tail area to Planform area (2*r*L)
AR_fin = 1;             % Aspect Ratio of fins (b^2/S)
findeflh0 = 0*(pi/180); % Fin deflection
finlimit = 45*(pi/180); % Fin deflection limit

%Moving Mass Characteristics
Wmm_W = 0.3;%*10^-6;
rpy_L = 0.0; rpz_L = r+1.75/2*.0254;

%Net buoyancy
B_W = 1.05;              %>1 for Buoyant <1 for Heavy
rho = 1025;%977.81;
g = 9.81;
```

```
%v = 0.9;

%%%%%%%%%%%%%%%%%%%%%%%%%%%%%%%%%%%%%%%%%%%%%%%%%%%%%%%%%%%%%%%%%%%%%%%%%%%%
n = 0;

%Elliptical craft winged Lift, Drag, Pitch Moment info
%Physical parameters
%Circular Cross section with wing span s from centerline
s = s_r*r; L = L_r*r;
Ab = pi*r^2;            %Stern Base Area
Ap = 2*r*L;             %Planform Area
Ar = Ap;                %Reference Area
%%%%%%%%%%%%%%%%%%%

xm = L/2; Vol = pi*r^2*L;
mbuoy = Vol*rho;    %Buoyancy in Kg
mb = (1/(B_W*(1+Wmm_W)))*mbuoy; mp = Wmm_W*mb; BmW = mbuoy-mb;

%Circular Cross section
CDn = 1.2; CA0 = 0.004; CNCN0SB = s_r^2+(1/s_r)^2-1;
CNCN0Newt = (3/2)*(s_r-(1/3)); CD0_hull = 0.002;

%Fin Properties
CLa_fin = pi*AR_fin/(1+sqrt(1+(AR_fin/2)^2)); V_tail = Lt_L*St_S;
St = St_S*Ar; CD0_fin = 0.006; e_fin = 1;

% Distances
xac = [(0.5-xac_L);0;zac_L]*L; rcg = [xcg_L;0;zcg_L]*L;
xt = [-L/2;0;0]; xv = [-L/2;0;0];
%rpx0 = -(1/Wmm_W)*xcg_L*L;
rpy = rpy_L*L; rpz = rpz_L*L;


% Inertia
Ib = diag([.5*mb*r^2,(1/12)*mb*L^2+0.25*mb*r^2,
        (1/12)*mb*L^2+0.25*mb*r^2]);

% Environment
```

```
g = 9.81;   % m/s^2
rho = 1025; % kg/m^3 - density

%Added Inertia
a = .75*L; b = r; ef = sqrt(1-(b/a)^2);
a0f = (2*(1-ef^2))/ef^3*(0.5*log((1+ef)/(1-ef))-ef);
b0f = 1/ef^2-(1-ef^2)/(2*ef^3)*log((1+ef)/(1-ef));
k1 = a0f/(2-a0f); k2=b0f/(2-b0f);
kp = (ef^4*(b0f-a0f))/((2-ef^2)*(2*ef^2-(2-ef^2)*(b0f-a0f)));

Jf = -diag([0,-kp*Ib(2,2),-kp*Ib(2,2)]);
Mf = -diag([-k1*mb,-k2*mb,-k2*mb]);


mt = mp+mb-mbuoy; findeflecth = 0;

alpha = -[1*pi/180:.01:80*pi/180];
%alpha = -30*pi/180;
for i = 1:length(alpha)
    beta(i) = 0;
    % Wing-Body Hydrodynamics
    CN(i) = -sign(alpha(i))*((Ab/Ar)*sin(2*abs(alpha(i)))
            *cos(abs(alpha(i)/2))*CNCN0SB+CDn*(Ap/Ar)
            *(sin(abs(alpha(i))))^2*CNCN0Newt);
    CA(i) = -CA0*(cos(alpha(i)))^2;
    CL(i) = CN(i)*cos(alpha(i))-CA(i)*sin(alpha(i));
    CD(i) = CN(i)*sin(alpha(i))+CA(i)*cos(alpha(i));
    Cm_wb(i) = sign(alpha(i))*(((Vol-Ab*(L-xm))
                /(Ar*L))*sin(2*abs(alpha(i)))
                *cos(abs(alpha(i)/2)))*CNCN0SB;
    %+(CDn*(Ap/Ar)*((xm-xac)/L)*sin(abs(alpha(i)))^2);

    % Fin Hydrodynamics
    if sin(alpha(i)) == 0;      CNf(i) = 0;
    else;  CNf(i) = sign(alpha(i))*(1/(0.222
            +(0.283/sin(alpha(i)-findeflecth))));
    end
    CAf(i) = -CD0_fin*cos(alpha(i))^2;
```

```
    CLf(i) = CNf(i)*cos(alpha(i))-CAf(i)*sin(alpha(i));
    CDf(i) = CNf(i)*sin(alpha(i))+CAf(i)*cos(alpha(i));

    if sin(beta(i)) == 0;      CNv(i) = 0;
    else;          CNv(i) = sign(beta(i))*(1/(0.222
                           +(0.283/sin(beta(i)))));
    end
    CAv(i) = -CD0_fin*cos(beta(i))^2;
    CLv(i) = CNv(i)*cos(beta(i))-CAv(i)*sin(beta(i));
    CDv(i) = CNv(i)*sin(beta(i))+CAv(i)*cos(beta(i));
    % Straight and Level Condition Glide path = 0
    theta(i) = alpha(i);

    % Determine Equilibrium Velocity
    qbar(i) = abs((mt*g*cos(theta(i)))
            /(CN(i)*Ar+CNf(i)*St));
    v(i) = sqrt(2*qbar(i)/rho);
    u(i) = v(i)*cos(alpha(i));
    w(i) = v(i)*sin(alpha(i));

    % Lift and Drag
    Lwb(i) = CL(i)*Ar*qbar(i);
    Dwb(i) = CD(i)*Ar*qbar(i);
    Mwb = Cm_wb(i)*Ar*L*qbar(i)*[0;1;0];
    Lt(i) = CLf(i)*St*qbar(i);
    Dt(i) = CDf(i)*St*qbar(i);
    Lv(i) = CLv(i)*St*qbar(i);
    Dv(i) = CDv(i)*St*qbar(i);



    % Rotation -beta about z, alpha about y
Raero = [ cos(alpha(i))*cos(beta(i)),
        -cos(alpha(i))*sin(beta(i)),
         -sin(alpha(i));
          sin(beta(i)),
          cos(beta(i)),
                      0;
```

```
      sin(alpha(i))*cos(beta(i)),
      -sin(alpha(i))*sin(beta(i)),
       cos(alpha(i));];

RT = [ cos(theta(i)), 0, -sin(theta(i));
    0,            1,             0;
    sin(theta(i)), 0, cos(theta(i));];
R = transpose(RT);

% Aero Forces
Faero = [ Dwb(i)+Dt(i)+Dv(i);
    Lv(i);
    Lwb(i)+Lt(i)];
Fb = Raero*Faero;

% Aero Moments
Mt = hat(xt)*Raero*[Dt(i);0;Lt(i)];
Mv = hat(xv)*Raero*[Dv(i);Lv(i);0];
Mw = hat(xac)*Raero*[Dwb(i);0;Lwb(i)];

% Gravitational Forces/moments
Fm = (mb+mp-mbuoy)*g*RT*[0;0;1];
Mcg = mb*g*hat(rcg)*RT*[0;0;1];

% Thrust
%T = -((CA(i)*Ar+CAv(i)*St)*qbar(i)
+mt*g*sin(theta(i)))*[1;0;0];
T = -(Fm(1)+Fb(1))*[1;0;0];

% Sum Forces/Moments
Fext = T + Fm + Fb;
Mext = Mt + Mv + Mw + Mcg + Mwb;% + hat(xt)*T;

%rpx(i) = (Mext(2))/(mp*g*cos(theta(i)))
-rpz*tan(theta(i));
%rpx(i) = (Mext(2)+mb*rcg(3)*u(i)-mb*rcg(1)
*w(i)+mp*rpz*u(i))/(mp*g*cos(theta(i)))+mp*w(i)
-rpz*tan(theta(i));
```

```
    rpx(i) = ((Mext(2)-(Mf(1,1)-Mf(3,3))*u(i)*w(i))
    /(mp*g*cos(theta(i))))-rpz*tan(theta(i));
    rp = [rpx(i);rpy;rpz];
    Mp = mp*g*hat(rp)*RT*[0;0;1];



end

% plot(alpha*(180/pi),CN)
% hold on
% plot(alpha*(180/pi),CA,'r--')
% xlabel('Angle of Attack, AoA, degrees')
% ylabel('Force Coefficient')
% legend('C_N','C_A',2)
% title('Comparison of Hull Normal &
Axial Force Coefficients')
%
% figure
% plot(alpha*(180/pi),CNf)
% hold on
% plot(alpha*(180/pi),CAf,'r--')
% xlabel('Angle of Attack, AoA, degrees')
% ylabel('Fin Force Coefficient')
% legend('C_{N_f}','C_{A_f}',2)
% title('Comparison of Hull Normal &
Axial Force Coefficients')

if length(alpha) > 1
    Dtotal = -(Dwb+Dt+Dv);
    Ltotal = Lwb+Lt;
    LoDtotal = Ltotal./Dtotal;
%     Dtotalmin = Dtotal(1);
%     for j = 1:length(Dtotal)
%         if Dtotal(j) <= Dtotalmin
%             Dtotalmin = Dtotal(j);
%             jmin = j;
%         end
```

```
%     end
[Dtotalmin,jmin] = min(Dtotal);
[LoDtotalmax,jLoDmax] = max(LoDtotal);

figure(1) hold on plot(alpha*(180/pi),v,'r:')
hold on plot(alpha(jmin)*(180/pi),v(jmin),'ro')
title('Equilibrium Angle of Attack and Velocity
Relation') xlabel('Angle of Attack,
AoA, degrees') ylabel('Velocity, v, m/s')

figure(2) hold on plot(alpha*(180/pi),rpx./L,'r:')
 hold on
 plot(alpha*(180/pi),0.4*ones(length(alpha)),'r--')
 plot(alpha*(180/pi),-0.4*ones(length(alpha)),'r--')
 title('Moving
Mass Position to Equilibrium AoA relation')
xlabel('Angle of Attack, AoA, degrees')
ylabel('Moving Mass Position, r_{p_x} /L')
legend('Moving Mass Position','Actuator Limits')

figure(3) hold on plot(v,rpx./L,'r:')
hold on plot(v,0.4*ones(length(alpha)),'r--')
plot(v,-0.4*ones(length(alpha)),'r--')
title('Moving Mass Position to Equilibrium Velocity
relation') xlabel('Velocity, v, m/s')
ylabel('Moving Mass Position, r_{p_x} /L')
legend('Moving Mass Position','Actuator Limits',4)

figure(4) hold on plot(v,Dtotal,'r:')
hold on plot(v(jmin),Dtotalmin,'ro')
xlabel('Velocity, v, m/s') ylabel('Drag')

figure(5) hold on plot(v,LoDtotal,'r:')
hold on plot(v(jLoDmax),LoDtotalmax,'ro')
xlabel('Velocity, v, m/s') ylabel('Lift/Drag')

figure(6) hold on plot(alpha*180/pi,LoDtotal,'r:')
hold on plot(alpha(jLoDmax)*180/pi,LoDtotalmax,'ro')
```

```
xlabel('Angle of Attack, AoA, degree')
ylabel('Lift/Drag') end
% figure
% plot(alpha*(180/pi),Mjorg)
% hold on
% plot(alpha*(180/pi),Mcg,'r:')
% plot(alpha*(180/pi),Mach,'g--')
% plot(alpha*(180/pi),Mht,'y')
% plot(alpha*(180/pi),MWa,'k-.')
% plot(alpha*(180/pi),MBa,'m')
% legend('Jorg','CG_B','AC_B','HT','CG_A','CB_A')
% title('Breakdown of Moments')
% xlabel('Angle of Attack, AoA, degrees')
%
%
% figure
% plot(alpha*(180/pi),(Cm./CNf)*2)
% title('Tail Area to Cancel Cm_{wb}')
% xlabel('Angle of Attack, AoA, degrees')
% ylabel('Tail Area Ratio, A_t/A_r')
%
% figure
% plot(alpha*(180/pi),(Cm./CNf))
% title('Tail Volume Ratio to Cancel Cm_{wb}')
% xlabel('Angle of Attack, AoA, degrees')
% ylabel('Horizontal Tail Volume ratio, \forall_t')
% % figure
% % plot(v,(Cm./CNf)*2)
%
% figure
% plot(alpha*(180/pi),(CN+CNf).*qbar.*Ar.*cos(theta))
% title('Equilibrium Lifting Force')
% xlabel('Angle of Attack, AoA, degrees')
% ylabel('Equilibrium Lifting Force')
%
% figure
% plot(v,(CN+CNf).*qbar.*Ar)
% title('Equilibrium Lifting Force')
```

```
% xlabel('Velocity, v, m/s')
% ylabel('Equilibrium Lifting Force')
%
% figure
% plot(v,(CN+CNf).*qbar.*Ar.*cos(theta))
% title('Equilibrium Lifting Force')
% xlabel('Velocity, v, m/s')
% ylabel('Equilibrium Lifting Force')
%
% figure
% plot(alpha*(180/pi),Cm.*qbar.*Ar*L)
% title('Destabilizing Wing-Body Pitching Moment')
% xlabel('Angle of Attack, AoA, degrees')
% ylabel('Wing-Body Pitching Moment, C_{m_{wb}}')
%
% figure
% plot(v,Cm.*qbar.*Ar*L)
% title('Destabilizing Wing-Body Pitching Moment')
% xlabel('Velocity, v, m/s')
% ylabel('Wing-Body Pitching Moment, C_{m_{wb}}')
%
% figure
% plot(alpha*(180/pi),Mht)
% title('Stabilizing Horizontal Tail Pitching Moment')
% xlabel('Angle of Attack, AoA, degrees')
% ylabel('Stabilizing Horizontal Tail Pitching Moment, C_{m_{ht}}')
%
% figure
% plot(v,Mht)
% title('Stabilizing Horizontal Tail Pitching Moment')
% xlabel('Velocity, v, m/s')
% ylabel('Stabilizing Horizontal Tail Pitching Moment, C_{m_{ht}}')

if length(alpha) == 1
%Inertia with Moving Mass
Inertiabm = [
    Ib-mp*hat(rp)^2,              mb*hat(rcg)+mp*hat(rp),
       mp*hat(rp)*e1;
```

```
    -mb*hat(rcg)-mp*hat(rp),     (mb+mp)*eye(3),
    mp*e1;
    -mp*transpose(e1)*hat(rp),   mp*transpose(e1),
    mp;
]; Inertiafl = -diag([0,-kp*Ib(2,2),-kp*Ib(2,2),
                -k1*mb,-k2*mb,-k2*mb,0]);

Inertia = Inertiabm+Inertiafl;
%invInertia = inv(Inertia);

v = [u(i);0;w(i)]; Omega = [0;0;0];

V = [Omega;v;0]; Pt = Inertia*V;

P = Pt(4:6); Pi = Pt(1:3); Pp = Pt(7);

PcV = hat(P)*v;

Pdot = hat(P)*Omega + Fext;
Pidot = hat(Pi)*Omega + PcV + Mext + Mp;


     fprintf('    [Pi;P;rp;Pp;R;xb;findelfh]   =
     [%4.4f;%4.4f;%4.4f;%4.4f;%4.4f;%4.4f;%4.4f;%4.4f;
     %4.4f;%4.4f;%4.4f;%4.4f;%4.4f;%4.4f;%4.4f;%4.4f;
     %4.4f;0;0;0;%4.4f]\n',Pt(1),Pt(2),Pt(3),Pt(4),Pt(5)
     ,Pt(6),rp(1),Pt(7),R(1,1),R(2,1),R(3,1),R(1,2),
     R(2,2),R(3,2),R(1,3),R(2,3),R(3,3),findeflecth)
 end
 vnorm = norm(v)
 %fprintf('Mt = %4.4f   Mv = %4.4f  Mw = %4.4f
 Mcg = %4.4f     Mwb = %4.4f     Mp = %4.4f
 PcV = %4.4f',Mt(2),Mv(2),Mw(2),Mcg(2),Mwb(2),Mp(2),PcV(2))
```

8.3 Parameter ID

```
clear close all clc

rho = 1025;

BmW = 3/100;        % 3 Percent Buoyant
L = 30      *.0254;             % Body Length in inches
r = 3.75/2  *.0254;

% Buoyancy and Weight
mb = 4.55;                      % Mass of AUV
mbuoyb = 1.03*pi*r^2*L*rho;     % Approximate Mass of
%displaced fluid (Cylinder volume +3% for nosecap and tailcap)
m_mma = 0.82;                % Mass of actuator
                             %without movable mass (kg)
mt = mb+m_mma;
mp = 0.8;                    % Mass of movable mass (kg)

rpz_L = 0.01; g = 9.81; qbar = .5*1025*1^2;
Ar = r^2*L; At_Ar = 0.3;

Cmcg = (mp*g)/(qbar*Ar);

Data = [2     1.50  -11.30  -4.47  10.08   11.72   -4.61 ;
        10     1.50  -9.81   -4.54  5.84    8.20    -1.09 ;
        20     1.50  -8.26   -5.05  4.33    4.02    3.09 ;
        30     1.50  -7.85   -6.16  -0.81   -2.66   9.76 ;
        40     1.50  -6.48   -5.44  -1.54   -5.76   12.86 ;
        50     1.50  -5.70   -6.72  -3.55   -8.28   15.38 ;
        60     1.54  -5.59   -8.58  -6.61   -11.15  18.26];

MMApos = Data(:,1);
Depth = Data(:,2);%*pi/180;
Pitch = Data(:,3);%*pi/180;
Roll = Data(:,4);%*pi/180;
Fin_a = Data(:,5);%*pi/180;
Fin_b = Data(:,6);%*pi/180;
```

```
Fin_c = Data(:,7);%*pi/180;

MMAposin = ((7.5/60)*MMApos-3.75)/L;
% Transorm MMA location to inches/L from CG/L
Fin_avg = (Fin_a+Fin_b)/2;

% A = [Pitch (Pitch+Fin_avg) Pitch zeros(7,3);
%     zeros(7,2) Pitch.*xt_L Pitch (Pitch+Fin_avg) MMAposin];
% A = [Pitch (Pitch+Fin_avg) Pitch zeros(7,3);
%     zeros(7,3) Pitch (Pitch+Fin_avg) MMAposin];
A = [Pitch 2*At_Ar*(Pitch+Fin_avg) Pitch zeros(7,2);
    zeros(7,3) Pitch At_Ar*2*(Pitch+Fin_avg)];


% B = [BmW*ones(7,1);0.000*ones(7,1)];
B = [BmW*ones(7,1);-(Cmcg*MMAposin+Cmcg*(rpz_L)*Pitch)];

format long; Coeff = pinv(A)*B;
CNthetawb = Coeff(1)
CNdeltae = Coeff(2)
CT = Coeff(3)
CMthetawb = Coeff(4)
CMdeltae = Coeff(5)
%CMdeltacg = Coeff(6)
format short;

% num = 7;
% A = [Pitch(1:num) (Pitch(1:num)+Fin_avg(1:num))
Pitch(1:num) zeros(num,3);
%     zeros(num,2) Pitch(1:num).*xt_L Pitch(1:num)
(Pitch(1:num)+Fin_avg(1:num)) MMAposin(1:num)];
%
% B = [BmW*ones(num,1);0.000*ones(num,1)];
% format long;
% Coeff = pinv(A)*B;
% CNthetawb = Coeff(1)
% CNdeltae = Coeff(2)
% CT = Coeff(3)
```

```
% CMthetawb = Coeff(4)
% CMdeltae = Coeff(5)
% CMdeltacg = Coeff(6)
% format short;
%
% (CNthetawb*Pitch+CNdeltae*(Pitch+Fin_avg)+CT*Pitch)-BmW
%
% CMthetawb*Pitch+CMdeltae*Fin_avg+CMdeltacg*MMAposin
```